Title: Antigen affinity, costimulation and cytokine inputs sum linearly to amplify T cell expansion

Authors: Julia M. Marchingo[1,2], Andrey Kan[1,2], Robyn M. Sutherland[1,2], Ken R. Duffy[3], Cameron J. Wellard[1,2], Gabrielle T. Belz[1,2], Andrew M. Lew[1,2], Mark R. Dowling[1,2,4], Susanne Heinzel[1,2]†, Philip D. Hodgkin[1,2]†*

Affiliations:

[1] Division of Immunology, The Walter and Eliza Hall Institute of Medical Research, Parkville, VIC, Australia.

[2] Department of Medical Biology, The University of Melbourne, Parkville, VIC, Australia.

[3] Hamilton Institute, National University of Ireland, Maynooth, Ireland.

[4] The Royal Melbourne Hospital, Parkville, VIC, Australia.

† These authors contributed equally to this work

* To whom correspondence should be addressed. Email: hodgkin@wehi.edu.au

Abstract: T-cell responses are initiated by antigen and promoted by a range of costimulatory signals. Understanding how T cells integrate alternative signal combinations and make decisions affecting immune response strength or tolerance poses a significant theoretical challenge. Here we report that T-cell receptor (TCR) and costimulatory signals imprint an early, cell-intrinsic, division fate, whereby cells effectively count through generations before returning automatically to a quiescent state. This autonomous program can be extended by cytokines. Signals from the TCR, costimulatory receptors and cytokines add together using a linear division calculus, allowing the strength of a T-cell response to be predicted from the sum of the underlying signal components. These data resolve a long-standing costimulation paradox and provide a quantitative paradigm for therapeutically manipulating immune response strength.

One Sentence Summary: T cells follow a linear calculus when integrating costimulatory and regulatory signals.

Main Text:

Upon infection pathogen-specific $CD8^+$ T cells undergo a characteristic kinetic sequence: rapid proliferation and expansion followed by population contraction due to cell death (*1*). While short-term stimulation is sufficient to trigger $CD8^+$ T-cell proliferation (*2, 3*) further exposure to stimulatory signals is required for an effective response (*2, 4, 5*). Although multiple attempts have been made to create a theory relating

the integration of stimulatory signals to T-cell response strength, all have been qualitative (*6*), and thus have lacked the power to predict the quantitative effect of altering stimulatory combinations and strength. The current qualitative paradigm describes T-cell activation and response magnitude as the outcome of 3 requisite signals: Signal 1) T-cell receptor (TCR) (*1*); Signal 2) membrane-bound antigen-presenting cell (APC)-delivered costimuli (*4*); and Signal 3) cytokines, from inflammatory, homeostatic or autocrine sources (*5*). The importance of these signals for T-cell expansion is highly context-dependent, as classic *in vitro* studies have identified many "critical" signal 2 and 3 molecules (*5, 7-9*); however, gene deletion typically yields only moderate defects in the *in vivo* $CD8^+$ T-cell response (*10-13*) implying considerable redundancy.

Recent studies in B cells report an automated return to quiescence after a series of division rounds (*14-16*). The number of mitotic cycles B cells undergo varies and is influenced by the strength of stimulation. We hypothesized that T cells might be programmed in a similar manner with the final number of divisions (*N*, Fig. 1A left panel) a function of the sum of inputs from signals 1-3 (illustrated Fig. 1A). If correct, it may be possible to determine the calculus of addition to serve as the basis for a quantitative framework for T cell costimulation.

To test this hypothesis we first measured the onset of quiescence in $CD8^+$ T cells using TCR-transgenic OT-I mice (which recognise SIINFEKL (N4) peptide bound to $H2K^b$) crossed with FucciRG mice in which cells fluoresce red (FucciR) during G_0/G_1 and green (FucciG) for the duration of $S/G_2/M$ (*17*). Quiescent ($FucciR^+G^-$), recently divided ($FucciR^-G^-$) and actively dividing ($FucciG^+$) cells can be distinguished, as cells that have reverted to a quiescent state (G_0) accumulate higher levels of FucciR (*17, 18*).

We define the number of generations of division before returning to quiescence as the cell's division destiny (DD) (*14-16, 19*). OT-I/FucciRG $CD8^+$ T cells were transferred into mice infected with recombinant HKx31 influenza virus expressing N4 (HKx31-N4) (*20*). During early expansion most OT-I/FucciRG $CD8^+$ T cells were proliferative, with <10% reverting to a quiescent state by day 3 of the response. This proportion of quiescent cells increased steadily reaching ~75% of all OT-I/FucciRG $CD8^+$ T cells by the onset of contraction at day 7 (Fig. 1B, C). To estimate the number of divisions T cells underwent before dropping out of cycle, the Cyton model (*15, 21*) was fitted to total and quiescent cell numbers (Fig 1D, Table S1). Results were consistent with a T-cell DD range spanning ~10 generations (Fig 1E). If clonal this predicts up to 1000-fold differences in descendant numbers from individual precursor cells, consistent with recent single-cell tracking studies (*22, 23*).

To further explore the regulation of division progression we developed a minimal *in vitro* stimulation system using CellTrace™ Violet (CTV) labeled OT-I/FucciRG T cells. The contribution of signals 2 and 3 was reduced by using peptide self-presentation by purified $CD8^+$ T cells (*24*). The strong effect of autocrine interleukin-2 (IL-2) was controlled by adding blocking antibody (clone S4B6) and using human IL-2 (hIL-2), resistant to S4B6, when required (*25*). Superficially the *in vitro* pattern of early proliferation with a gradual onset of quiescence recapitulated the *in vivo* response (Fig. 1C, F), with the major differences being the DD and subsequent time to die (Fig. 1D, E, G, Table S1).

We speculated that the three known sources of regulation, TCR affinity, costimuli and cytokines might combine to convert the low DD observed *in vitro* into the extensive outcome possible *in vivo* (Fig. 1E).

To improve estimation of mean DD (mDD) in our CTV division tracking assay we used OT-I T cells deficient in the pro-apoptotic molecule Bim (OT-I/*Bcl2l11*$^{-/-}$) for all experiments. These cells reported the same mDD as OT-I/*Bcl2l11*$^{+/+}$ T cells (Fig. 2A, S1A-C, Table S2) but the enhanced survival upon reverting to quiescence facilitated DD measurement at later times, consistent with previous studies in B cells (*15, 16*).

Fig. S2A-F shows the effect of a range of T cell stimuli on mDD. TCR affinity, several agonists representative of cell-contact mediated costimulation and some, but not all, cytokines tested were able to regulate DD in a dose dependent manner. To determine when DD was most susceptible to regulation, cells from cultures where stimulation was removed immediately prior to the first division (*24*) were compared to cells with constant costimulation. Anti-CD28 and anti-CD27 principally acted prior to the first division. In contrast, ongoing exposure to IL-2, IL-4 and IL-12 was required for maximal proliferation (Fig. 2B). Higher levels of IL-2 or IL-4 caused T cells to divide beyond CTV resolution (Fig. S3) and the culture capacity. Therefore, to investigate the potential of IL-2 and IL-4 to extend DD when cytokine levels were maintained, OT-I/*Bcl2l11*$^{-/-}$ CD8^{+} T cells were sub-cultured every 48 hours in hIL-2 (Fig. 2C) or IL-4 (Fig. S4A) and total cell numbers calculated using splitting ratios. Cyton fitting revealed that hIL-2 and IL-4 can increase the mDD by up to ~11 and 7 divisions respectively (Fig. 2C-E, S4A, B, Table S3, S4). Titration of hIL-2 showed the effect on mDD to be dose dependent (Fig. 2D) and that this increase in mDD was associated with an increase in variance (Fig. 2E,

Fig. S4C). Together these results demonstrated that DD can be intrinsically programmed by early signals, but also has the flexibility to be 'reprogrammed' or extended by extrinsic stimuli as the T cells divide.

We then determined how T cells integrated multiple contributors to DD. In Figure 3A and B we show the increase in mDD imprinted prior to the first division for low concentrations of the individual costimuli anti-CD28, anti-CD27 and IL-12. The combination of anti-CD28 and anti-CD27 programmed a mDD that was equivalent to the sum of each individual effect, with IL-12 giving a slightly greater than additive increase in mDD (Fig. 3C, D). Importantly, no single 'second signal' appeared obligatory, but rather multiple small arithmetic effects on DD culminated in large geometric differences in the cell numbers produced (Fig. 1A center and right panels). Thus, an increase of~2.2 divisions in mDD (Fig. 3D) with the accompanying ~0.5 division increase in standard deviation (Fig. S5A-D, Table S5) summed from three weak costimuli resulted in a net ~8-fold increase in the peak cell number (Fig. 3E, F), with the additional difference in response magnitude attributable to small variations in the starting cell number (Fig S5E, Table S5). Early programming was cell intrinsic as cells imprinted with a mDD of ~1 or ~3.4 generations gave the same outcome irrespective of whether they were subsequently cultured separately or together (Fig. S6A, B). The approximately additive effect of stimuli on DD also applied for a range of combinations when stimuli were retained in culture during subsequent division rounds (Fig. S7A-D).

Taken together this series of experiments reveals two stages of regulation of T cell DD. In the first stage, signal 1 and a series of signal 2 and 3 stimuli of different strengths and combinations can additively 'program' a heritable number of division

rounds prior to the first cell division. In the second stage, exposure to external signals, mainly cytokines, can be processed and added to the DD. These features are consistent with a molecular mechanism whereby each stimulatory signal contributes a quantum of mitosis promoting protein or complex that is diluted by division until a sub-mitotic concentration is reached and division ceases (*26*).

The two-stage DD programming model makes two key predictions for the role of extrinsic factors, such as IL-2, that could be tested during *in vivo* $CD8^+$ T-cell responses: i) the major physiological role of autocrine IL-2 is in maintaining division and therefore it will be more important away from the initial site of $CD8^+$ T-cell priming and ii) the effect of IL-2 on DD will sum with other stimuli allowing the prediction of T cell expansion kinetics when IL-2 and other stimuli are combined.

We tested the first prediction by comparing the expansion of IL-2 receptor α deficient OT-I T cells (OT-I/*Il2ra*$^{-/-}$) with OT-I/*Il2ra*$^{+/+}$ $CD8^+$ T cells in two different *in vivo* systems, namely an anti-influenza response and islet graft rejection model. Similar numbers of OT-I/*Il2ra*$^{+/+}$ and OT-I/*Il2ra*$^{-/-}$ $CD8^+$ T cells were detected at the site of priming (mediastinal lymph node, mLN) during the expansion phase when co-transferred into HKx31-N4 infected mice (Fig. 4A). In contrast, a bias towards expansion of OT-I/*Il2ra*$^{+/+}$ $CD8^+$ T cells was observed in the spleen and lungs, consistent with a role for IL-2 in the maintenance of cell expansion (Fig 4A). OT-I/*Il2ra*$^{+/+}$ $CD8^+$ T cells also outcompeted OT-I/*Il2ra*$^{-/-}$ $CD8^+$ T cells at the effector site during an anti-islet graft response (Fig 4B). The proportion of $BrdU^+$ OT-I/*Il2ra*$^{+/+}$ $CD8^+$ T cells after a 1 hour *in vivo* BrdU pulse was ~2.5 times greater than for OT-I/*Il2ra*$^{-/-}$ $CD8^+$ T cells in the graft

(Fig. 4C) confirming this bias was attributable to proliferation in the effector site and not due to migration alone (*27*).

To investigate the additive nature of T-cell stimuli *in vivo,* OT-I/*Il2ra*$^{+/+}$ and OT-I/*Il2ra*$^{-/-}$ CD8^{+} T cells were co-transferred into mice infected with either high (HKx31-N4) or low (HKx31-Q4) affinity influenza virus (*20*). The Cyton model was fitted to T-cell numbers to estimate the increase in DD due to TCR affinity or IL-2 signaling alone (Fig. 4D, E top, Table S6). By summation of these individual contributions to the mean and variance of the DD distribution we predicted the effect of a combined increase in TCR affinity and IL-2 signaling on DD (Fig. 4E, bottom) and successfully recreated the expansion kinetics of OT-I/*Il2ra*$^{+/+}$ T cells during an HKx31-N4 infection (Fig. 4F).

Manipulating T-cell responses via costimulation and cytokine signaling is an important emerging therapeutic regimen (*28, 29*) and a quantitative framework will facilitate the rational development of optimal interventions. To support this goal we propose a quantitative paradigm where no one signal is obligatory but rather combinations of inputs add together to geometrically enhance outcomes (Fig. 1A). Thus combinations of different costimulatory and cytokine signals provide many alternative paths to generate T-cell responses of similar magnitude. This framework reconciles long-standing discrepancies between *in vivo* and *in vitro* results for IL-2 and costimulatory signals and reveals a quantitative basis for current switch-inspired two- and three-signal models of activation. Further studies measuring simultaneous differentiation changes to effector and memory states associated with cell division would complete the T-cell calculating framework and further enhance our ability to predict therapeutic strategies for immunomodulation.

References and Notes:

1. D. Zehn, S. Y. Lee, M. J. Bevan, Complete but curtailed T-cell response to very low-affinity antigen. *Nature* **458**, 211 (2009).
2. S. M. Kaech, R. Ahmed, Memory CD8+ T cell differentiation: initial antigen encounter triggers a developmental program in naïve cells. *Nat. Immunol.* **2**, 415 (2001).
3. M. J. van Stipdonk, E. E. Lemmens, S. P. Schoenberger, Naïve CTLs require a single brief period of antigenic stimulation for clonal expansion and differentiation. *Nat. Immunol.* **2**, 423 (2001).
4. E. M. Bertram, W. Dawicki, T. H. Watts, Role of T cell costimulation in anti-viral immunity. *Sem. Immunol.* **16**, 185 (2004).
5. J. M. Curtsinger *et al.*, Inflammatory cytokines provide a third signal for activation of naive CD4+ and CD8+ T cells. *J. Immunol.* **162**, 3256 (1999).
6. A. G. Baxter, P. D. Hodgkin, Activation rules: the two-signal theories of immune activation. *Nat. Rev. Immunol.* **2**, 439 (2002).
7. D. A. Cantrell, K. A. Smith, The interleukin-2 T-cell system: a new cell growth model. *Science* **224**, 1312 (1984).
8. L. A. Gravestein, J. D. Nieland, A. M. Kruisbeek, J. Borst, Novel mAbs reveal potent co-stimulatory activity of murine CD27. *Int. Immunol.* **7**, 551 (1995).
9. F. A. Harding, J. G. McArthur, J. A. Gross, D. H. Raulet, J. P. Allison, CD28-mediated signalling co-stimulates murine T cells and prevents induction of anergy in T-cell clones. *Nature* **356**, 607 (1992).
10. T. R. Malek, The biology of interleukin-2. *Annu. Rev. Immunol.* **26**, 453 (2008).
11. A. Oxenius, U. Karrer, R. M. Zinkernagel, H. Hengartner, IL-12 Is Not Required for Induction of Type 1 Cytokine Responses in Viral Infections. *J. Immunol.* **162**, 965 (1999).
12. A. Shahinian *et al.*, Differential T cell costimulatory requirements in CD28-deficient mice. *Science* **261**, 609 (1993).
13. K. P. J. M. van Gisbergen *et al.*, The costimulatory molecule CD27 maintains clonally diverse CD8(+) T cell responses of low antigen affinity to protect against viral variants. *Immunity* **35**, 97 (2011).
14. E. D. Hawkins, J. F. Markham, L. P. McGuinness, P. D. Hodgkin, A single-cell pedigree analysis of alternative stochastic lymphocyte fates. *Proc. Natl. Acad. Sci. U.S.A* **106**, 13457 (2009).
15. E. D. Hawkins, M. L. Turner, M. R. Dowling, C. van Gend, P. D. Hodgkin, A model of immune regulation as a consequence of randomized lymphocyte division and death times. *Proc. Natl. Acad. Sci. U.S.A* **104**, 5032 (2007).

16. M. L. Turner, E. D. Hawkins, P. D. Hodgkin, Quantitative regulation of B cell division destiny by signal strength. *J. Immunol.* **181**, 374 (2008).

17. M. R. Dowling *et al.*, Stretched cell cycle model for proliferating lymphocytes. *Proc. Natl. Acad. Sci. U.S.A* **111**, 6377 (2014).

18. M. Tomura *et al.*, Contrasting quiescent G0 phase with mitotic cell cycling in the mouse immune system. *PLoS ONE* **8**, e73801 (2013).

19. Materials and methods are available as supplementary materials on Science Online.

20. A. E. Denton *et al.*, Affinity thresholds for naive CD8+ CTL activation by peptides and engineered influenza A viruses. *J. Immunol.* **187**, 5733 (2011).

21. E. D. Hawkins *et al.*, Quantal and graded stimulation of B lymphocytes as alternative strategies for regulating adaptive immune responses. *Nat. Commun.* **4**, 2406 (2013).

22. V. R. Buchholz *et al.*, Disparate Individual Fates Compose Robust CD8+ T Cell Immunity. *Science* **340**, 630 (2013).

23. C. Gerlach *et al.*, Heterogeneous Differentiation Patterns of Individual CD8+ T Cells. *Science* **340**, 635 (2013).

24. M. Hommel, P. D. Hodgkin, TCR affinity promotes CD8+ T cell expansion by regulating survival. *J. Immunol.* **179**, 2250 (2007).

25. E. K. Deenick, A. V. Gett, P. D. Hodgkin, Stochastic model of T cell proliferation: a calculus revealing IL-2 regulation of precursor frequencies, cell cycle time, and survival. *J. Immunol.* **170**, 4963 (2003).

26. As OT-I division times are relatively homogeneous a division based dilution model is difficult to distinguish from a mechanism where the loss of division motivation ceases in all descendants at a nominated time after activation. Further molecular studies are needed to test between these, and other possible mechanisms.

27. W. Weninger, M. A. Crowley, N. Manjunath, U. H. von Andrian, Migratory Properties of Naive, Effector, and Memory CD8+ T Cells. *J. Exp. Med.* **194**, 953 (2001).

28. M. Dougan, G. Dranoff, Immune therapy for cancer. *Annu. Rev. Immunol.* **27**, 83 (2009).

29. G. Kinnear, N. D. Jones, K. J. Wood, Costimulation blockade: current perspectives and implications for therapy. *Transplantation* **95**, 527 (2013).

30. G. T. Belz, L. Zhang, M. D. H. Lay, F. Kupresanin, M. P. Davenport, Killer T cells regulate antigen presentation for early expansion of memory, but not naive, CD8+ T cell. *Proc. Natl. Acad. Sci. U.S.A* **104**, 6341 (2007).

31. M. Liu, M. E. Shapiro, A new method for isolation of murine islets with markedly improved yields. *Transplant. Proc.* **27**, 3208 (1995).

32. V. G. Subramanian, K. R. Duffy, M. L. Turner, P. D. Hodgkin, Determining the expected variability of immune responses using the cyton model. *J. Math. Biol.* **56**, 861 (2008).

Acknowledgments: We thank S. Turner for providing the recombinant influenza virus and discussion and comments on the manuscript; L. Corcoran and V. Bryant for discussion and comments on the manuscript; A.Giang for discussion of experiments; M. Camilleri, L. Mackiewicz, M. Dayton and D. Pavlyshyn for technical assistance; and P. Bouillet for *Bcl2l11*$^{-/-}$ mice; Fucci Red and Fucci Green mice were provided by the Riken BioResource Centre through the National BioResource Project of the Ministry of Education, Culture, Sports, Science and Technology-Japan. We also thank K. Lafferty and his two signal theory for inspiring this work. The data are tabulated in the main paper and in the supplementary materials. Experimental data and the code for fitting the Cyton model will be made available upon request. This work was supported by the National Health and Medical Research Council via project Grant 1010654 &1043414, program Grants 1054925 & 1037321, and fellowships to M.R.D., A.M.L. and P.D.H. as well as Independent Research Institutes Infrastructure Support Scheme Grant 361646. K.R.D and P.D.H were supported by Human Frontier Science Program grant RGP0060/2012, G.T.B. was supported by an Australian Research Council Future Fellowship and K.R.D. was supported by Science Foundation Ireland Grant 12IP1263. This work was made possible through Victorian State Government Operational Infrastructure Support and Australian Government NHMRC IRIISS. J.M.M. was the recipient of an Australian Postgraduate Award and WEHI Edith Moffat Scholarship.

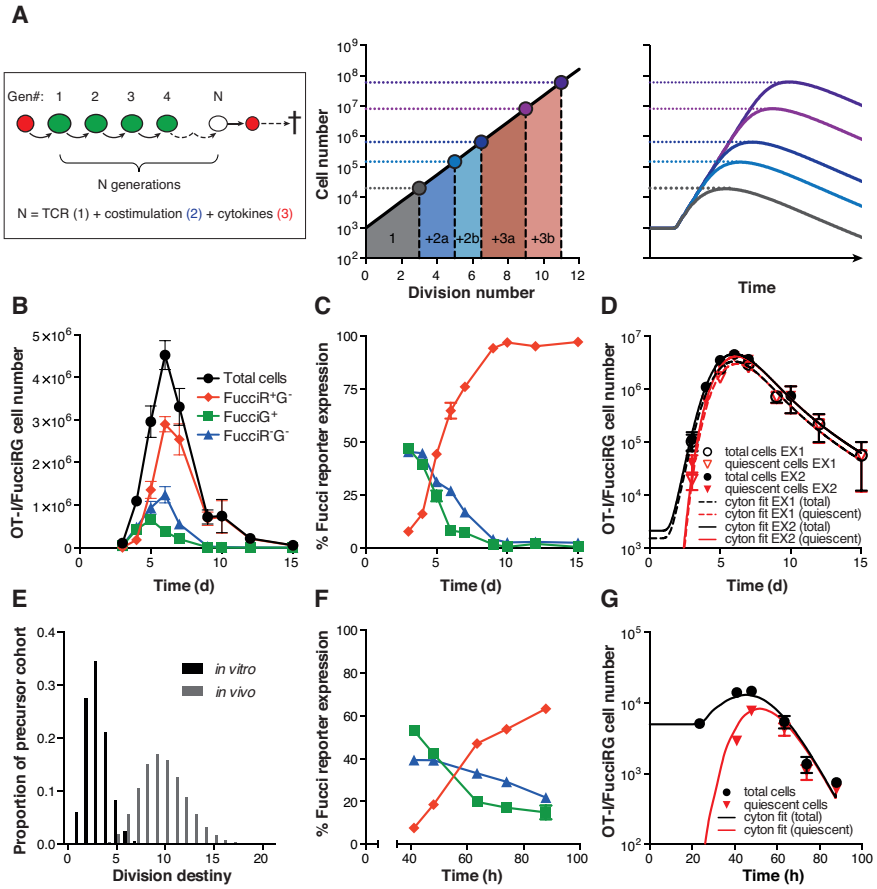

Fig. 1. CD8$^+$ T cells undergo a program of proliferation and quiescence *in vivo* and *in vitro*. (**A**) Quantitative T cell expansion hypothesis. By this model the number of mitotic cycles a T cell undergoes following activation (N) varies, and is determined by a sum of the individual inputs it receives. In the example shown signal 1, 2 and 3 stimuli each individually elicit a small increase in mean population division number. The cumulative effect of these contributions, when summed linearly, would lead to geometric increases in total cell number at the peak response. Analysis of OT-I/FucciRG CD8$^+$ T cells (B-E) transferred to HKx31-N4 infected recipients on day 2 post-infection or (E-G) *in vitro* stimulated with N4 in the presence of mIL-2 blocking antibody (S4B6). (**B**) Number and (**C**) percentage of OT-I/FucciRG CD8$^+$ T cells expressing FucciR and FucciG reporter proteins pooled from mediastinal lymph node, spleen and lungs at the indicated time-points post-transfer. (**D**) Fitted total (black) and quiescent (red, FucciR$^+$G$^-$ + small FucciR$^-$G$^-$ cells) cell numbers using the Cyton model(*19*). (**E**) The estimated DD distribution from Cyton fitting to *in vivo* (D) and *in vitro* (G) stimulated cells. (**F**) Percentage of FucciR and FucciG expression. (**G**) Fitted total (black) and quiescent (red, FucciR$^+$G$^-$ + small FucciR$^-$G$^-$ cells) cell numbers(*19*). (B-E) n= 5-10 mice/time-point pooled from 2 independent experiments: Mean ± SEM. (E-G) Representative of 3 independent experiments: Mean ± SEM from triplicate culture wells.

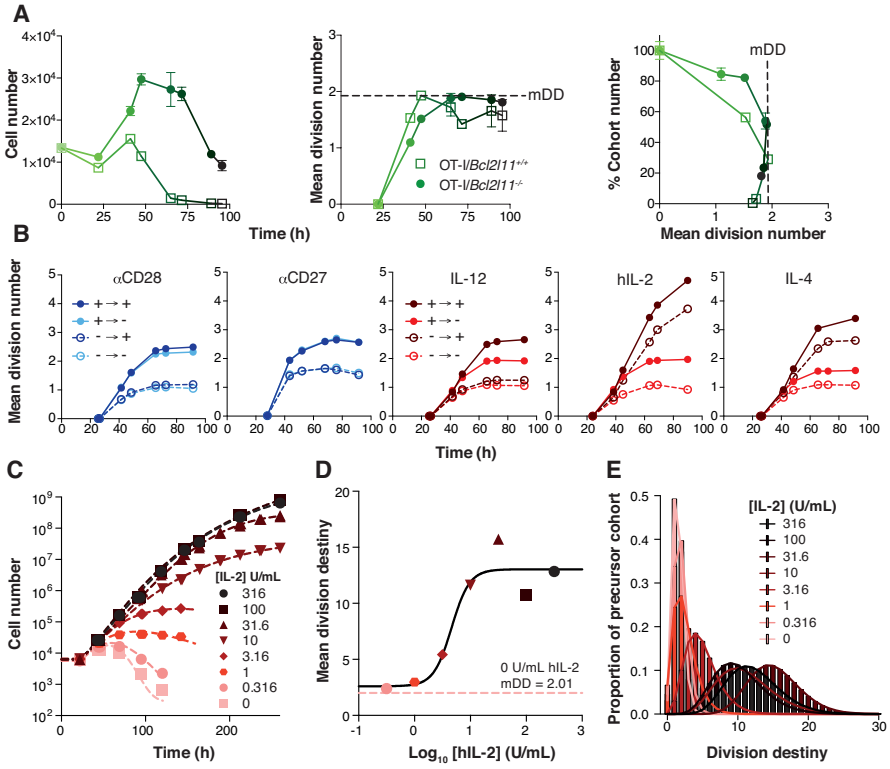

Fig. 2. Costimuli and cytokines program changes to DD. (**A**) CTV-labeled OT-I/*Bcl2l11*$^{+/+}$ or OT-I/*Bcl2l11*$^{-/-}$ CD8^{+} T cells were stimulated with N4; total cell numbers (left), mean division number (middle) and an estimation of the percentage of the starting cells whose progeny are contributing to the response at that time-point, calculated by removing the effect of cell expansion at each time-point (percent cohort number, right; as described in (*19*)) were determined. Mean DD (mDD) on each graph is indicated by dotted lines. (**B**) Mean division number of CTV-labeled OT-I/*Bcl2l11*$^{-/-}$ CD8^{+} T cells cultured in the presence (+, solid lines) or absence (-, dotted lines) of αCD28 (2 µg/mL), immobilized αCD27 (5 µg/mL), IL-12 (1 ng/mL), human IL-2 (hIL-2, 31.6 U/mL) or IL-4 (1000 U/mL) for 26 hrs, washed and further cultured with (dark) or without (light) costimulation. (**C**) CTV-labeled OT-I/*Bcl2l11*$^{-/-}$ CD8^{+} T cells stimulated with N4 in the presence of hIL-2 at the indicated concentrations were subcultured into fresh hIL-2 every ~48 hrs and cell number was fitted using the Cyton model (dotted lines)(*19*). (**D**) Dose response curve of mDD and (**E**) DD distributions from Cyton fitting in (C). All cultures contained 25 µg/mL S4B6. Representative of at least 2 independent experiments: Mean ± SEM from triplicate culture wells.

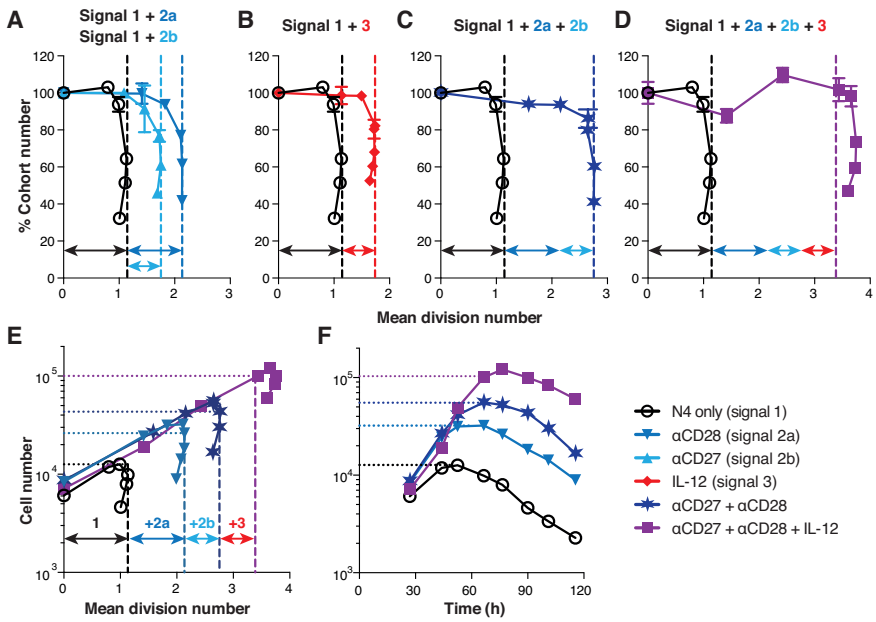

Fig. 3. Summation of DD from multiple costimuli geometrically amplifies the T-cell response. Percentage cohort number (see Fig. 2A and (*19*)) *vs.* mean division number for N4 stimulated CTV-labeled OT-I/*Bcl2l11*$^{-/-}$ CD8^{+} T cells cultured with (**A**) immobilized anti-CD27(5 µg/mL), anti-CD28 (2 µg/mL) or (**B**) IL-12 (1 ng/mL) alone, **(C)** immobilized anti-CD27 and anti-CD28 together, or (**D**) a combination of all 3 costimuli for 26 hrs, washed and recultured without further stimulation. Relationship between cell number and either (**E**) mean division number or (**F**) time for data in (A-D). Arrows represent the effect of individual stimuli on mDD. All cultures contained S4B6 at 25 µg/mL Graphs are representative of 3 independent experiments. Mean ± SEM of triplicate culture wells.

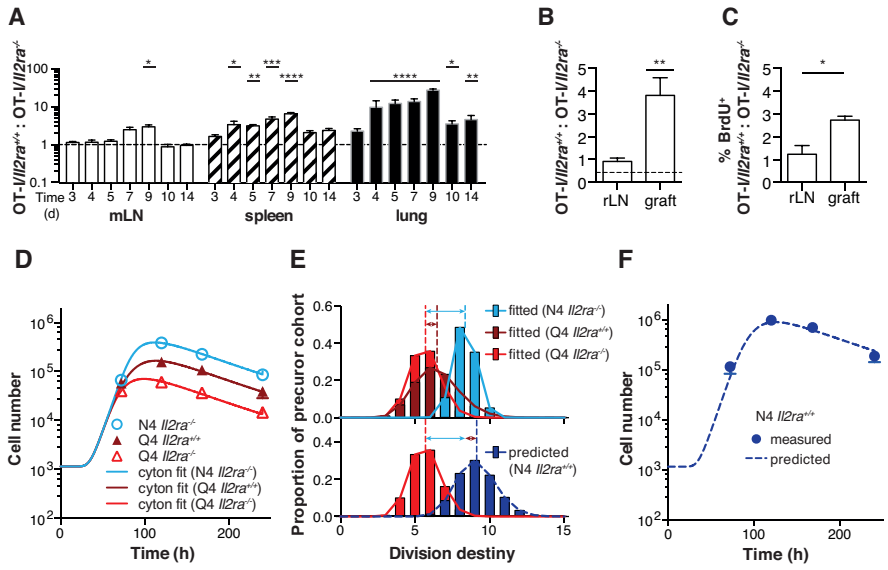

Fig. 4. IL-2 sums with TCR-affinity to determine T cell expansion. (**A**) Ratio of OT-I/*Il2ra*$^{+/+}$:OT-I/*Il2ra*$^{-/-}$ CD8^{+} T cells recovered from mLN, spleen and lungs after co-transfer of equal numbers of each into HKx31-N4 infected recipients. Mean ± SEM, n= 5-10 mice/time-point pooled from 2 independent experiments: Two-way ANOVA. (**B**) Ratio of OT-I/*Il2ra*$^{+/+}$:OT-I/*Il2ra*$^{-/-}$ of divided CD8^{+} T cells and (**C**) divided %BrdU^{+} CD8^{+} T cells from renal (draining) lymph node (rLN) and graft for CTV-labeled OT-I/*Il2ra*$^{+/+}$ and OT-I/*Il2ra*$^{-/-}$ CD8^{+} T cells co-transferred to recipient mice at a 30:70 ratio 1 day prior to engraftment with RIP-mOVA islets under the renal capsule. Mice were pulsed with BrdU 1 hr before organ harvesting on day 6 post-graft. Mean ± SEM, n= 4 mice, representative of 2 independent experiments: Two-way ANOVA and one-tailed t-test respectively. For all experiments data points were excluded from ratio and % calculations when less than 100 cells were detected. Dotted lines in (A) and (B) represent the OT-I/*Il2ra*$^{+/+}$:OT-I/*Il2ra*$^{-/-}$ transfer ratio. (**D**) The Cyton model was fitted to OT-I/*Il2ra*$^{+/+}$ and OT-I/*Il2ra*$^{-/-}$ T cell numbers from HKx31-Q4 infected mice and OT-I/*Il2ra*$^{-/-}$ T cells from HKx31-N4 infected mice pooled from the mLN, spleen and lungs after co-transfer of equal numbers of cells into recipient mice and (**E**) the division destiny distribution was determined (top)(*19*). By summation of mean and variance of these DD distributions the cumulative effect of increasing TCR-antigen affinity and IL-2 signaling on the DD distribution (i.e. the DD distribution for OT-I/*Il2ra*$^{+/+}$ T cells in HKx31-N4 infected mice) was predicted (bottom) (**F**) Using this mean and variance the cell number over time was predicted for OT-I/*Il2ra*$^{+/+}$ T cells in HKx31-N4 infected mice(*19*). Mean ± SEM n= 5 mice/time-point, representative of 2 independent experiments. For all statistics asterisks denote p< **** 0.0001, *** 0.001, ** 0.01 or * 0.05.

Supplementary Materials:

www.sciencemag.org

Materials and Methods

Figures S1-S10

Tables S1-S9

References (*30*-*32*)

Supplementary Materials for

Antigen affinity, costimulation and cytokine inputs sum linearly to amplify T cell expansion

Julia M. Marchingo, Andrey Kan, Robyn M. Sutherland, Ken R. Duffy, Cameron J. Wellard, Gabrielle T. Belz, Andrew M. Lew, Mark R. Dowling, Susanne Heinzel, Philip D. Hodgkin

correspondence to: hodgkin@wehi.edu.au

This PDF file includes:

Materials and Methods:

Mice:

Bcl2l11$^{-/-}$ (B6.129S1-*Bcl2l11*$^{tm1.1Ast}$) mice were a gift from Philippe Bouillet (WEHI), *Il2ra*$^{-/-}$ (B6;129S4-*Il2ra*^{tm1Dw}/J) mice were obtained from The Jackson laboratory and Fucci Red mice (B6.B6D2-Tg(FUCCI)596Bsi) were bred with Fucci Green mice (B6.B6D2-Tg(FUCCI)504Bsi), both obtained from the Riken BioResource Centre (Hirosawa, Wako, Saitama, Japan) to create FucciRG mice. FucciRG, *Bcl2l11*$^{-/-}$ and *Il2ra*$^{-/-}$ mice were bred with OT-I (C57B6-Tg(TcraTcrb)1100Mjb) mice from the WEHI animal facility (Kew, Victoria, Australia) to create OT-I/FucciRG (*17*), OT-I/*Bcl2l11*$^{-/-}$ and OT-I/*Il2ra*$^{-/-}$ strains. RIP-mOVA (C57BL/6-Tg(Ins2-TFRC/OVA)296Wehi/Wehi), OT-I/CD45.1, OT-I/CD45.1 × C57BL/6 F1 (OT-I/CD45.1/CD45.2) donor mice and CD45.1 and CD45.1 × C57BL/6 F1 (CD45.1/CD45.2) recipient mice were obtained from the WEHI animal facility. All mice were bred and maintained under specific pathogen-free conditions in the WEHI animal facilities (Parkville, Victoria, Australia) and used between 6-14 weeks of age. All experiments were performed under the approval of the WEHI Animal Ethics Committee.

CD8$^+$ T cell preparation:

CD8$^+$ T cells were isolated from mouse lymph nodes (inguinal, axillary, brachial, superficial cervical and lumbar) or spleens by negative selection using either the Mouse CD8α$^+$ T cell isolation kit II (Miltenyi) or EasySep Mouse CD8$^+$ T cell Isolation kit (StemCell Technologies) according to the manufacturer's protocols. Enrichment of OT-I CD8$^+$T cells was confirmed by flow cytometry with a yield of 85-95% CD8$^+$Vα2$^+$ lymphocytes. For cell proliferation assays CD8$^+$ T cells were labeled with 5 μM CellTrace Violet (CTV) or 5 μM CFSE (both from Invitrogen) where stated according to manufacturer instructions.

In vitro cell culture:

CD8$^+$T cells were cultured in RPMI 1640 medium (Invitrogen) supplemented with non-essential amino acids, 1 mM Sodium-pyruvate, 10 mM HEPES, 100 U/ml Penicillin, 100 μg/ml Streptomycin (all Invitrogen), 50μM 2β-mercaptoethanol, 2 mM L-glutamine (both Sigma) and 10% FCS (JRH Biosciences and Invitrogen). OT-I CD8$^+$ T cells were stimulated with SIINFEKL (N4) peptide or the lower affinity peptide variant SIIGFEKL (G4) (both from Auspep) in 96 well round-bottomed plates by self-presentation (*24*) at a density of 10,000 cells/well in 200 μL complete tissue culture medium. All cultures contained 25 μg/mL of anti-mouse IL-2 monoclonal antibody (supernatant from hybridoma cell line S4B6, WEHI) which blocks the activity of mouse IL-2 *in vitro* but does not recognise human IL-2 (hIL-2)(*25*). Recombinant hIL-2 (Peprotech), recombinant murine IL-4 (baculovirus-transfected Sf21 insect cell supernatant, WEHI), recombinant murine IL-12 (R&D Systems), recombinant murine IL-21 (Immunex), recombinant murine IL-6 (purified from transfected COS cell supernatant, DNAX), recombinant murine IFN-γ (Genzyme), recombinant murine IL-10 (purified from baculovirus-transfected Sf21 insect cell supernatant, DNAX), anti-CD28 (clone 37.51, WEHI monoclonal antibody facility) were added to cultures where indicated. In cultures containing anti-CD27 (BD, NA/LE clone LG-3A10) plates were coated overnight and antibody washed off prior to culture, as cross-linking is required to elicit stimulatory activity. Cells were incubated in a humidified environment at 37^{o}C in 5% CO_2.

Influenza infections:

Recipient mice were anaesthetized with methoxyflurane then infected intranasally with 10^4 pfu of recombinant influenza virus HKx31 encoding the chicken ovalbumin peptide SIINFEKL (HKx31-N4) or the lower affinity variant SIIQFEKL (HKx31-Q4) (*20*). On day 2 post infection at the approximate peak of antigen presentation in the mediastinal lymph node (mLN) (*30*) 10^5 purified CTV labeled OT-I/FucciRG or 5×10^4 OT-I/*Il2ra*$^{+/+}$ and 5×10^4 OT-I/*Il2ra*$^{-/-}$ (ratio 50:50) CD8$^+$ T cells were adoptively transferred intravenously into the tail vein. At the time-points indicated, mLNs, spleen and lungs were harvested and mashed through 70 μm strainers to produce single cell suspensions. For mLNs and spleens a red blood cell lysis was performed prior to staining. For lungs, mononuclear cells were enriched by centrifugation for 18 minutes 2000 rpm at room temperature on a Histopaque density gradient (1.077 g/mL, Sigma) prior to staining. Transferred viable cells (fixable viability dye negative) were identified according to their expression of CD8, CD45.1, CD45.2 and Vα2.

Estimating quiescent cell numbers *in vivo*:

Cells that have returned to a quiescent state can be identified by the accumulation of FucciRed protein to a high level over time in the Fucci system (*17, 18*) but are notably also smaller in size (Fig. S8A, D) (*14*). As the FucciRed reporter takes time to accumulate, using FucciR$^+$G$^-$ cells alone to estimate the number of quiescent cells would result in an underestimate. To gain a more accurate measurement of the number of quiescent cells at a given time-point during the OT-I/FucciRG response we defined total quiescent cell number as the sum of FucciR$^+$G$^-$ cells plus the FucciR$^-$G$^-$ cells which were considered small based upon their FSC/SSC profile (i.e. the cell predicted to up-regulate FucciRed protein after sufficient time spent in G_0) (Fig. S8B, C, E, F). These numbers were used with total cell number for Cyton model fitting (described below).

Islet grafts/*in vivo* BrdU labeling:

0.6×10^6 OT-I/*Il2ra*$^{+/+}$ and 1.4×10^6 OT-I/*Il2ra*$^{-/-}$ (ratio 30:70) CD8$^+$ T cells were intravenously adoptively transferred into recipient mice 1 day prior to engraftment under the kidney capsule with 400 RIP-mOVA islets. Islets were isolated by Collagenase P digestion and Histopaque-1077 density gradient centrifugation (*31*) then hand-picked and counted prior to grafting. On day 6 post-graft, mice were injected with 200 μL BrdU (6.25 mg/mL in PBS) i.p. 1 hour prior to euthanasia. The renal lymph node and graft were harvested and digested with frequent mixing at room temperature in 1mg/ml Type III Collagenase (Worthington) and 0.01% w/v Grade II bovine pancreatic DNAse I (Roche) for 30 minutes with addition of EDTA at a final concentration of 8mM for the final 5 minutes. Detection of intracellular BrdU was performed using BrdU staining kit (BD Pharmingen) as per manufacturer instructions. Transferred viable cells (fixable viability dye negative) were identified according to their expression of CD8, CD45.1, CD45.2 and Vα2.

Flow cytometry, Cell Counting and Cell surface/viability dye staining:

Flow Cytometry was performed on FACSCanto II cytometer (BD Biosciences). Data was analyzed using FlowJo software (Treestar).

A known number of beads (SPHERO Nile Red, Blank or Rainbow calibration particles or CaliBRITE FITC beads, all BD Biosciences) were added to samples immediately prior to analysis and the ratio of beads to live cells was used to calculate the absolute cell number in each sample (*24*). Propidium iodide (0.2 μM, Sigma) or fixable viability dye eFluor780 (concentration 1/1000) (eBioscience) were used for dead cell exclusion for *in vitro* and *in vivo* experiments, respectively.

The following monoclonal antibodies were used for the detection of cell surface markers: anti-CD8α-FITC, -APC-Cy7 (clone 53-6.7), anti-Vα2-PE, -PerCPCy5.5 (clone B20.1) anti-CD45.2-PE-Cy7, -APC (clone 104) (all BD Biosciences), anti-CD8α-PE-Cy7 (clone 53-6.7) anti-CD45.2-FITC (clone 104) (both eBioscience) and anti-CD45.1-BV650 (A20, BioLegend).

For islet graft experiments, cells were incubated in FcR block (2 ug of 2.4G2 FcγIII/II mAb) for 10 minutes on ice prior to staining. Antibody and fixable viability dye eF780 staining were performed simultaneously.

Division Destiny:

Division destiny (DD) is used to characterize cell proliferation systems where cells divide for a series of generations then return to a quiescent non-dividing state (*14-16*). The final generation reached is termed the cell's division destiny and it may have been set within, and inherited from, an antecedent cell. For this concept we assume cells carry a division register and descendant cells count down as necessary until the programmed destiny is reached. We note two influences over DD: 1) Founder cells can be programmed for different DD prior to first division, and 2) activated dividing blasts can be 'reprogrammed' by external signals and the inherent DD register further altered. If all cells underwent the same number of divisions following stimulation (e.g., all progeny divided N times and then entered the quiescent state) then DD (and the average, mDD) would be equal to that number (e.g., DD = mDD = N). In practice, however, DD is a random variable for a population of cells, and the mean and variance of this variable must be estimated from experimental data. We note two alternative calculations of mDD. First, is to treat destiny as principally family tree-based and calculate the average generation depth of the range of family trees. Thus, mDD is then calculated from data where the effect of cell expansion is removed by dividing the number of cells in generation i by 2^i yielding precursor cohort numbers (*24*). The second interpretation treats all cells as independent and the average generation of all cells calculated (*16*). This method skews the average DD to higher values as the variance increases. As our primary interest is in the priming of DD in founder cells we adopt the first interpretation.

We develop two analytical methods for estimating the mDD from data, one based on precursor cohort numbers and the other based on Cyton modeling. Where possible we use the precursor cohort method as it makes few assumptions and is computationally efficient. However, this method is constrained by the resolution of cell tracking dyes, as it requires cell numbers per division data. Where only total cell numbers are known or we seek an estimate of the DD variance we use the Cyton method.

Precursor Cohort Based Method:

The precursor cohort method first removes the effect of cell division on the total cell numbers (*24*). For each time-point, the number of cells in a given division *i* was converted to a precursor cohort number (C_i) using the following formula:

$$C_i = \frac{cell\ number\ in\ division\ i}{2^i}. \qquad (1)$$

Note that undivided cells are said to be in division *i=0*. In some cases cohort number is percentage normalized (calculated from a time-point typically between 20-30 hours after stimulation). If there is no cell death or loss, the sum of cohort numbers from each generation will always equal the precursor cell number. Thus, reduction in this number indicates death and loss of either precursors or their descendants.

A maximum number of 7-8 divisions can be traced using cell division tracking dyes such as CTV and CFSE. For a given time-point, the cohort numbers estimate a distribution that characterizes the number of divisions progeny cells underwent by this time-point. The mean of this distribution is called *mean division number* and is estimated as:

$$mean\ division\ number = \frac{\sum_{k=0}^{K} k \cdot C_k}{\sum_{k=0}^{K} C_k}. \qquad (2)$$

Here *K* is the number of divisions that can be resolved. Assuming little cell death, this mean division number will increase over time as cells progress through divisions and reach a plateau at mDD. The mDD using the cohort method is therefore defined as the maximum mean division number calculated in this way over all the measured time-points.

Cyton Modeling:

The Cyton model of lymphocyte proliferation assumes each cell has autonomous molecular machinery governing division and death set in competition (*15, 21*). Mathematically, times for division and death are represented as independent, division-dependent random variables, with the earlier of the two determining the fate of the cell. The model assumes both division and death times are reset upon division, so that new times for division and death are drawn for the next division cycle measured from the previous division time. The model incorporates division destiny by counting generations and once destiny is reached and division switched off, death becomes the winning and inevitable consequence. Here we use the model (*15, 21*) with a few modifications outlined below.

First, we write out the equations of the original Cyton model using slightly different notation to the original. For the data presented in this paper, the starting cell number, N_0, is large enough that it is sufficient to consider the mean number of cells in each division, without regard to the variance (*32*). Let $N_i(t)$ be the mean number of cells in division i at time, t. Let $p_i^{div}(t)$ and $p_i^{die}(t)$ be probability distributions for division and death of cells in division i, respectively (below we assign specific parameterized probability distributions). Let $P_i^{div}(t) = \int_o^t p_i^{div}(\tau) \cdot d\tau$ and $P_i^{die}(t) = \int_o^t p_i^{die}(\tau) \cdot d\tau$ be the corresponding cumulative distributions. Let ψ_i be the progressor fraction for cells in division i (i.e. the proportion of the cell population that enter generation *i* that are motivated to divide into generation *i*+1 (*15, 21*), defined below in terms of the division

destiny distribution). For undivided cells ($i = 0$), the instantaneous rates of division, $n_0^{div}(t)$, and death, $n_0^{die}(t)$ are given by:

$$n_0^{div}(t) = N_0 \cdot \psi_0 \cdot \left(1 - P_0^{die}(t)\right) \cdot p_0^{div}(t), \quad (3)$$

$$n_0^{die}(t) = N_0 \cdot \left(1 - \psi_0 \cdot P_0^{div}(t)\right) \cdot p_0^{die}(t). \quad (4)$$

For subsequent divisions ($i \geq 1$), the instantaneous rates of division and death are determined by the integral equations:

$$n_i^{div}(t) = 2 \cdot \psi_i \cdot \int_0^t n_{i-1}^{div}(\tau) \cdot \left(1 - P_i^{die}(t-\tau)\right) \cdot p_i^{div}(t-\tau) d\tau, \quad (5)$$

$$n_i^{die}(t) = 2 \cdot \int_0^t n_{i-1}^{div}(\tau) \cdot \left(1 - \psi_i \cdot P_i^{div}(t-\tau)\right) \cdot p_i^{die}(t-\tau) d\tau. \quad (6)$$

The total rates of change of mean cell numbers are defined by a set of ordinary differential equations:

$$\frac{dN_o(t)}{dt} = -n_0^{div}(t) - n_0^{die}(t), \quad (7)$$

$$\frac{dN_i(t)}{dt} = 2n_{i-1}^{div}(t) - n_i^{div}(t) - n_i^{die}(t), \quad (8)$$

with initial conditions, $N_0(0) = N_0$, $N_i(0) = 0, i \geq 1$.

The model also determines the number of quiescent cells over time, allowing fits to this additional data component, which was not considered in previous work. The change in number of quiescent cells from division i , $N_i^{qui.}(t)$, over time as follows:

$$\frac{dN_0^{qui}(t)}{dt} = -(1 - \psi_0) \cdot N_0 \cdot p_0^{die}(t), \quad (9)$$

$$\frac{dN_i^{qui}(t)}{dt} = 2 \cdot (1 - \psi_i) \cdot \left(n_{i-1}^{div}(t) - \int_0^t n_{i-1}^{div}(\tau) \cdot p_i^{die}(t-\tau) d\tau\right), \quad (10)$$

with initial conditions, $N_0^{qui}(0) = (1 - \psi_0) \cdot N_0$, $N_i^{qui}(0) = 0, i \geq 1$.

The original description of the Cyton model presented a general framework that allows any distribution for division destiny, and for the fitting we chose a truncated normal distribution (*15*). However, here we found that a long tailed distribution provided a superior fit to OT-I/*Bcl2l11*$^{-/-}$ CD8$^+$ T cells which had been stimulated to reach DD within the resolution of CTV (Fig. S9A, Table S7). Both discretized gamma and lognormal distributions greatly improved estimates. However, as long as division outcompetes death on average, a discretized lognormal distribution for DD will result in an infinite expansion in mean cell number (Fig. S9B, Table S8) (*32*). By contrast, with a suitable parameterization of the discretized gamma distribution the infinite expansion is avoided. This point is illustrated in Figure S9B, which shows the extrapolation of the fit to cell numbers using either discretized lognormal or gamma DD. With a discretized lognormal DD the population is predicted to continue to grow, whilst with discretized gamma DD the predicted to plateau, despite very similar fits to the earlier measured time-

points. We therefore use the discretized gamma distribution for DD. In summary, the discretized probability distribution, f_i, for DD with parameters (α, β) in our version of the Cyton model is defined as

$$f_i = \int_i^{i+1} f_{gam}(x)\, dx, \qquad (11)$$

where the gamma probability density function is

$$f_{gam}(x) = \frac{\beta^\alpha}{\Gamma(\alpha)} x^{\alpha-1} e^{-\beta x}, x > 0, \qquad (12)$$
$$f_{gam}(0) = 0.$$

We define the cumulative DD, F_i, up to and including division *i*, as

$$F_i = \sum_{k=0}^{i} f_k. \qquad (13)$$

The progressor fraction, ψ_i for division $i > 0$, is defined to be the conditional probability that a cell's division destiny is greater than *i*, given that it is known to be greater than *i-1*.

$$\psi_i = \frac{1-F_i}{1-F_{i-1}}, \qquad (14)$$

while for *i*=0

$$\psi_0 = \mathrm{R}_0(1 - f_0),$$

where R_0 is the fraction of responding naive cells.

Parameter Estimation Strategy:

The formulation of the Cyton model used has six independent modules described by 12 parameters:

1. *Initial cell number* (N_0) and *responding fraction* (R_0)
2. *Time to first division* (lognormal, μ_0^{div}, σ_0^{div})
3. *Time to death, first division* (lognormal, μ_0^{die}, σ_0^{die})
4. *Time to subsequent divisions* (lognormal, μ_{1+}^{div}, σ_{1+}^{div})
5. *Time to death, subsequent divisions* (lognormal, μ_{1+}^{die}, σ_{1+}^{die})
6. *Division destiny* (discretized gamma, μ^{DD},σ^{DD}, which uniquely define parameters (α, β) as above)

Where FucciRG reporter information was available the Cyton model was fit to all live and quiescent cell numbers. When this information was unavailable, the model was fit to live cell numbers only. When CTV dilution data was available (i.e. *in vitro* proliferation <~90hrs) the cyton model was fit to cell number per division. In conditions where CTV was fully diluted (i.e. *in vitro* >~90hrs and *in vivo* > day 3 post-transfer) cells

were classified as being in the maximum detectable division or higher for cyton fitting. All conditions within an experiment were fitted simultaneously.

Given a dataset for each condition the task to identify the values for the 12 model parameters followed these consecutive steps:

1. Identify parameters that can be locked on a value and those that must be varied.
2. Identification of *a priori* feasible parameter ranges to constrain the parameters to be varied.
3. Define an objective function that characterizes the discrepancy between model predictions and observed data.
4. Use an optimization algorithm to find parameter values that minimize the discrepancy.

In the first step, we applied the following parameter constraints:

Initial cell number, responding fraction and death prior to first division:

1) For *in vitro* experiments the initial cell number was determined as the cell number measured at a time-point just prior to entry into first division. For *in vivo* experiments cohort numbers were estimated on day 3 of the response (when CTV dilution profiles were still resolvable) as described above. In these experiments initial cell number was constrained to remain between the minimum and maximum cohort numbers determined.
2) There was near complete recruitment of OT-I T cells into the first division allowing responding fraction to be set to 1. Death prior to the first division was negligible in all experiments and was therefore removed from the model.

These two steps reduced the number of free fitting parameters to 8 for *in vitro* and 9 for *in vivo* experiments.

Mean time to first division, subsequent division rate:

3) For *in vitro* sub-culturing experiments (Fig. 2C-E, S4) the model was initially fit to time-points where CTV was incompletely diluted (i.e. <~90hrs) to estimate μ_0^{div}, σ_0^{div} and μ_{1+}^{div}. These values were locked in and then the model was fit to the complete data set.
4) For *in vivo* experiments the mean and standard deviation of time to first division was estimated by fitting an inverse cumulative lognormal to the percentage of undivided cells (Fig. S10) as described previously (*23*).
5) The variance of subsequent division times can be poorly constrained by fitting if few time-points contain CTV information. Filming experiments determined the variance of log(division time) for OT-I T cells as 0.14 (*17*) and this value was used for all experiments with time-points in which cells proliferated beyond the resolution of CTV.

These steps reduced the number of free fitting parameters to 6 for *in vivo* experiments and 4 when fitting to the complete data set for *in vitro* sub-culturing experiments.

Constraints between conditions:

6) When fitting to *in vivo* replicate experiments (Fig 1D) all parameters were fixed to be constant between replicates except for initial cell number which was estimated to be significantly different between experiments (two-tailed student t-test, p=0.039).
7) When fitting to data of the *in vivo* response to varying affinity and *Il2ra* expression (Fig. 4D-F) the initial cell number was fixed to be constant across all conditions as there was no significant difference in the initial cell numbers between conditions (one-way ANOVA, p=0.82). Subsequent division rate was constrained to be constant across all conditions based on previous studies (*24*). Linear regression analysis of log-transformed cell number after peak response revealed no difference in rate of cell loss between conditions during the contraction phase (ANCOVA, p=0.68). Therefore, cell death rate was held to be constant between conditions to allow estimation of cell expansion based upon the predicted DD distribution.
8) When fitting to IL-2 titration data (Fig 2C) the mean and standard deviation for time to first and subsequent divisions were fixed to be constant across all conditions based upon previous studies (*24, 25*).

For our objective function, we used the weighted sum of squared residuals as described previously (*21*).

$$W = \sum_{i,j,k} \frac{\left(n_{i,j,k} - y_{i,j}\right)^2}{y_{i,j} + \varepsilon}, \qquad (15)$$

where n denotes measured cell numbers, y the model prediction, i, j and k indices the division number, time-point and replicate respectively and ε the variance intercept, which can be thought as a lower bound for the variance of experimental noise. Previously, this intercept was heuristically estimated using measured data (*21*). However, we could not use the same estimation method as this heuristic method gave us large negative numbers for some datasets. Therefore, we used another method which is also based on the measured data. As the measured data comprise multiple replicates, we computed sample variances for each of the replicate groups. We then considered this set of estimated variances as a set characteristic of the dataset, and set ε to θ percentile of this set (this could be set to the minimum observed variance, but it is more reliable to set it to a small percentile). Here θ was a user-specified threshold and we tested threshold values of 0.25, 0.5, 1, 2, and 4 and found little difference in fitting results (Table S9). We therefore used a θ value of 1.

Finally, we used an interior point optimization algorithm implemented in the *fmincon* function of MATLAB (MathWorks, version 2012 and higher). This algorithm requires a starting guess for parameter values, and we used 30 random starting sets. In each starting set, each starting parameter value was drawn uniformly at random from the identified parameter ranges. These starting sets resulted in 30 fits that could be sorted by quality using the objective function described above. We then identified the best fit, and repeated it, but each time using an artificial dataset resampled with replacement from the original measured data. This process was repeated 30 times, resulted in 30 estimates for

each parameter, and allowed us to estimate confidence intervals on estimated parameter values.

Additive prediction of DD distribution mean and variance:

To predict the mean or variance (when an estimate of the variance is available) of the DD distribution programmed by multiple costimuli in combination (Fig. 3A-D, Fig S5A-D) the mean and variance of the DD distribution of the cells without costimulation (N4 only) was subtracted from the mean and variance DD of the anti-CD27, anti-CD28 and IL-12 conditions to give the mean and variance above baseline for the DD distributions of each individual costimulus. For each costimulation combination the mean and variance of the DD distribution was predicted by addition of the mean and variance above baseline for the relevant costimuli to the mean and variance of DD distribution for the N4 only condition.

To estimate the DD distribution resulting from an increase in TCR-antigen affinity and IL-2 signaling *in vivo* (Fig. 4D-F) OT-I/*Il2ra*$^{-/-}$ CD8^{+} T cells in HKx31-Q4 infected mice was taken to be the baseline condition. The change in mean and variance of DD compared to baseline due to TCR-antigen affinity and IL-2 signaling was determined by subtraction of the mean and variance of the baseline condition from the mean and variance of the DD distribution estimated from cyton fitting to OT-I/*Il2ra*$^{-/-}$ T cells in HKx31-N4 infected mice and OT-I/*Il2ra*$^{+/+}$ T cells in HKx31-Q4 infected mice respectively. To predict the DD distribution for OT-I/*Il2ra*$^{+/+}$ in HKx31-N4 infected mice the increase in mean and variance above baseline for affinity and IL-2 signaling was summed with the mean and variance of the baseline DD distribution.

Statistics, linear regression analysis and fitting the IL-2 dose response curve:

The following statistics and curve fitting was performed in PRISM software (GraphPad). Ratios of OT-I/*Il2ra*$^{+/+}$ and OT-I/*Il2ra*$^{-/-}$ in flu infection and islet graft experiments (Fig. 4A, B) were compared to the transfer ratio using a two-way ANOVA on log-transformed data with a Sidak post-test. A one-tailed student t-test was used to determine whether %BrdU incorporation of OT-I/*Il2ra*$^{+/+}$ and OT-I/*Il2ra*$^{-/-}$ CD8^{+} T cells was greater in the graft compared to the rLN (Fig. 4C). Data points were excluded from ratio calculations and statistical tests when fewer than 100 cells were detected. A two-tailed t-test was used to test if the initial cell number calculated for Fig. 1D was the same between replicate experiments. A one-way ANOVA was used to test if initial cell number calculated in Fig. 4D was equal across groups. To compare death rates in Fig 4D T-cell numbers for day 5 or later (i.e. the contraction phase) were log-transformed and a linear regression analysis performed. An ANCOVA was used to test if the slopes differed between conditions. IL-2 concentrations were log transformed and mDD data fitted with a sigmoidal 4PL curve. Line of best fit for plots of variance *vs.* mDD was determined using a linear regression analysis.

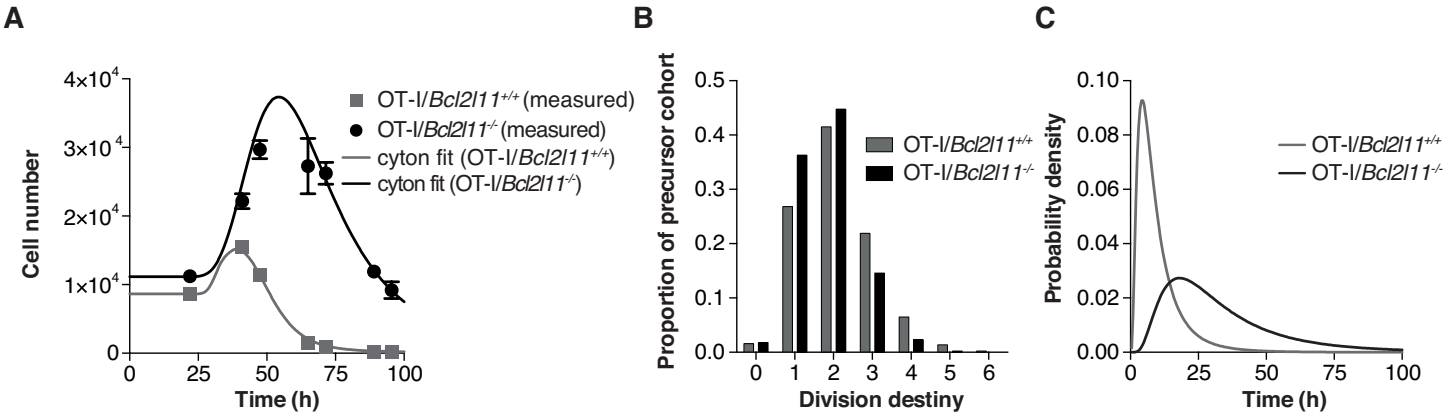

Fig. S1. OT-I/*Bcl2l11*$^{-/-}$ CD8$^+$ T cells have the same DD but a delayed time to die compared to OT-I/*Bcl2l11*$^{+/+}$ CD8$^+$ T cells.
CTV-labeled OT-I/*Bcl2l11*$^{+/+}$ or OT-I/*Bcl2l11*$^{-/-}$ CD8$^+$ T cells were stimulated with N4 in the presence of S4B6. (**A**) The Cyton model was fitted to cell number and the effect of Bim deficiency (encoded by *Bcl2l11*) on (**B**) DD distribution and (**C**) time to die in division 1$^+$ was estimated. Representative of 2 independent experiments. Mean ± SEM from triplicate culture wells.

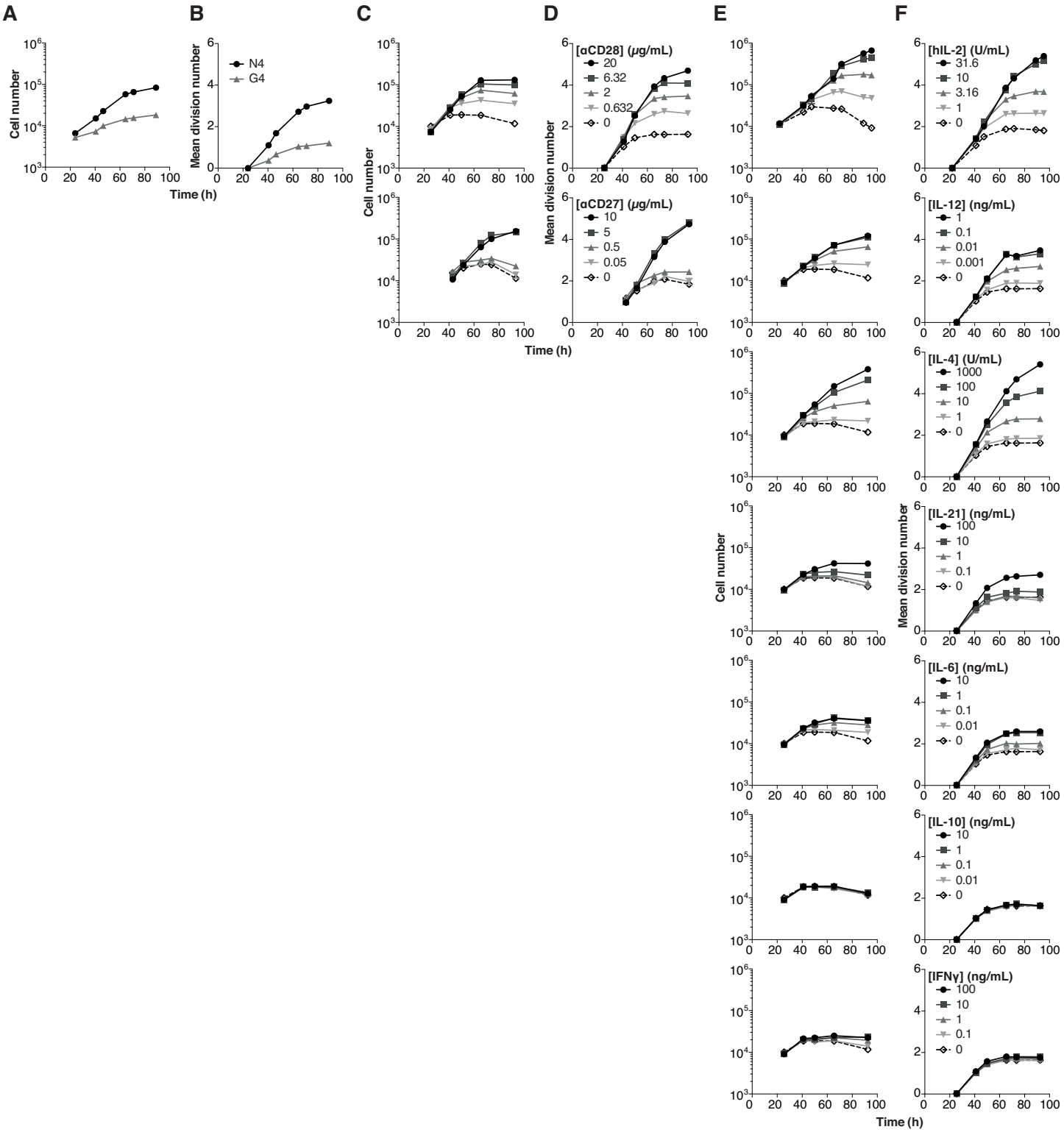
A
B
C
D
E
F
Cell number
Mean division number
Time (h)
N4
G4
[αCD28] (μg/mL)
20
6.32
2
0.632
0
[αCD27] (μg/mL)
10
5
0.5
0.05
0
[hIL-2] (U/mL)
31.6
10
3.16
1
0
[IL-12] (ng/mL)
1
0.1
0.01
0.001
0
[IL-4] (U/mL)
1000
100
10
1
0
[IL-21] (ng/mL)
100
10
1
0.1
0
[IL-6] (ng/mL)
10
1
0.1
0.01
0
[IL-10] (ng/mL)
10
1
0.1
0.01
0
[IFNγ] (ng/mL)
100
10
1
0.1
0

Fig. S2. Quantitative programming of DD by TCR affinity and various signal 2 and 3 costimuli.

(A, C, E) Total cell number and (B, D, F) mean division number were measured over time for CTV-labeled OT-I/*Bcl2l11*$^{-/-}$ CD8^{+} T cells when stimulated with (**A,B**) N4 (0.01 μg/mL, K_d= 6.5 μM) or G4 (0.1 μg/mL, K_d= 10.0 μM) (*24*) peptide in the presence of 3.16 U/mL hIL-2 or N4 peptide plus representative (**C, D**) contact-dependent costimuli or (**E, F**) APC or inflammation-derived cytokines at the concentrations indicated. All cultures contained 25 μg/mL S4B6. Mean ± SEM from triplicate culture wells, representative of 2-3 independent experiments.

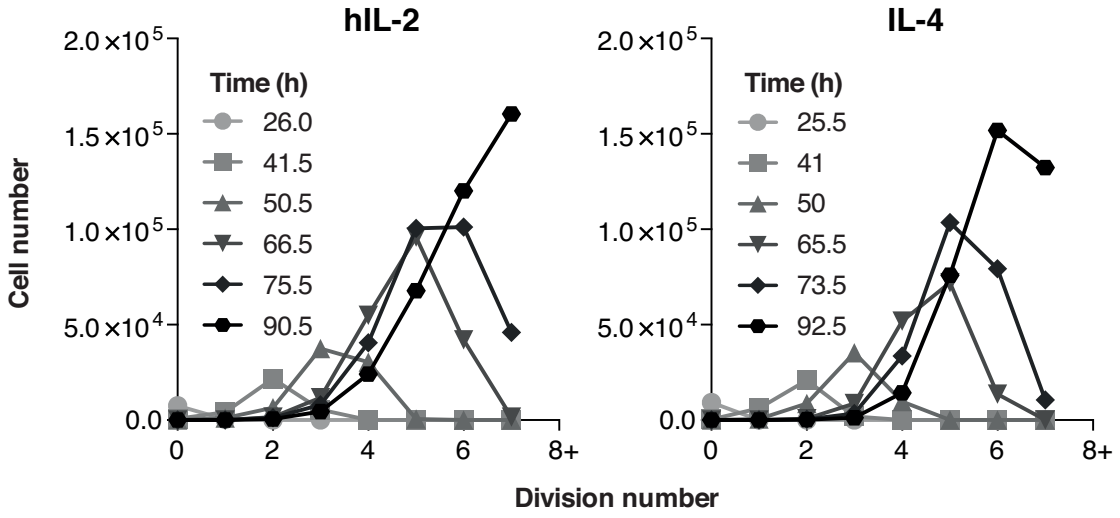

Fig. S3. High concentrations of hIL-2 and IL-4 drive proliferation beyond CTV resolution.

Cell number per division was measured at various time-points for CTV-labeled OT-I/*Bcl2l11*$^{-/-}$ CD8^{+} T cells stimulated with N4 peptide in the presence of 25µg/mL S4B6 and high doses of hIL-2 (left, 31.6 U/mL) or IL-4 (right, 1000 U/mL). Mean ± SEM from triplicate culture wells, representative of 2 independent experiments.

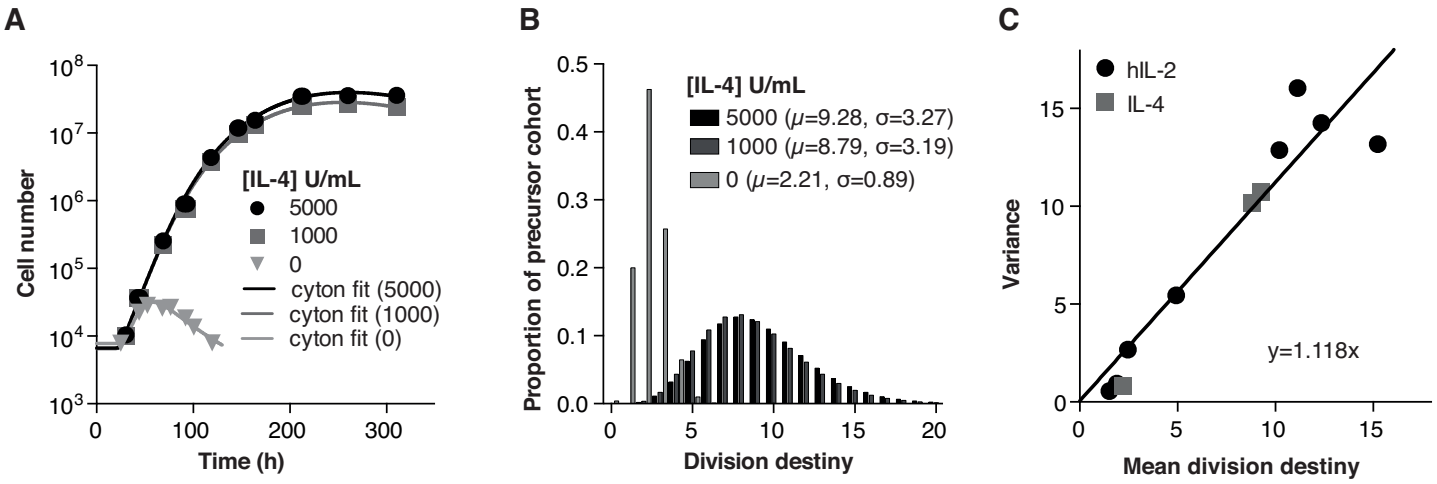

Fig. S4. Maintenance of high levels of IL-4 extends DD.
(**A**) CTV-labeled OT-I/*Bcl2l11*$^{-/-}$ CD8^{+} T cells stimulated with N4 in the presence of IL-4 at the indicated concentrations were sub-cultured into fresh IL-4 every ~48 hrs and cell number was fitted using the Cyton model (*19*). Mean ± SEM from triplicate culture wells. (**B**) DD distribution from cyton fits in (A). (**C**) Variance *vs.* mean of the DD distributions from cyton fitting in (A) and in Fig. 2C. All cultures contained 25 μg/mL S4B6. Representative of 2 independent experiments.

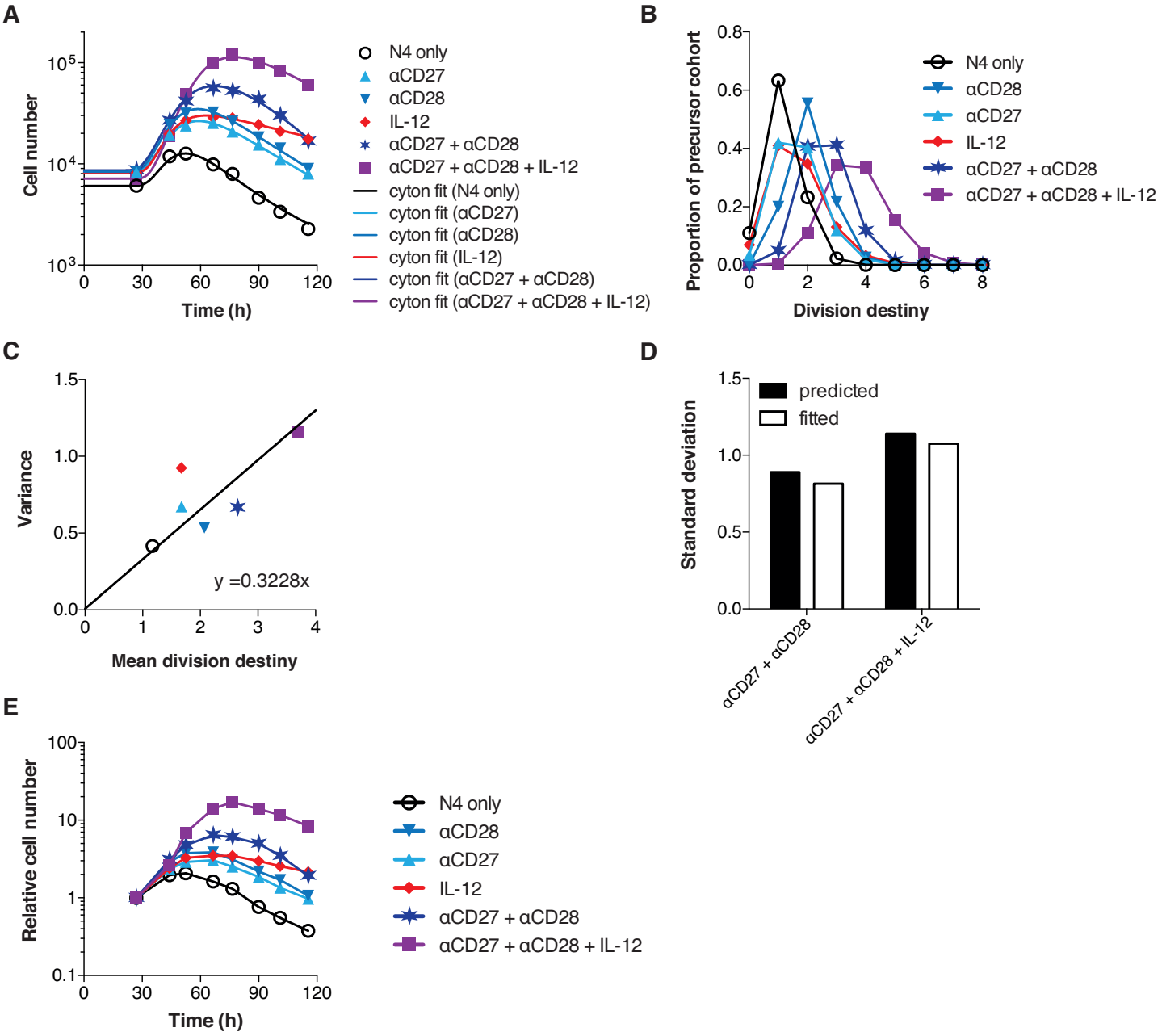

Fig. S5. Combined costimuli program an additive increase in DD.
OT-I/*Bcl2l11*$^{-/-}$ CD8^{+} T cells were stimulated with N4 and cultured in the presence of immobilized anti-CD27, anti-CD28 and IL-12 (5 µg/mL, 2 µg/mL, and 1 ng/mL respectively) alone or in combination for 26 hrs, washed and re-cultured in complete tissue culture media without stimuli. (**A**) Total cell number per division was fitted using the Cyton model (*19*) and the effect of individual and combined costimuli on (**B**) DD distribution was estimated. (**C**) Variance *vs.* mean of DD distributions from Cyton fit in (A). (**D**) Variance of DD distributions for costimuli combinations was predicted by summation of the differences in DD distribution variances of individual costimuli (*19*) and compared to variances estimated from cyton fitting in (A). (**E**) Total cell number per time-point normalized to starting cell number. All cultures contained S4B6 at 25 µg/mL. Representative of 3 independent experiments, Mean ± SEM from triplicate culture wells.

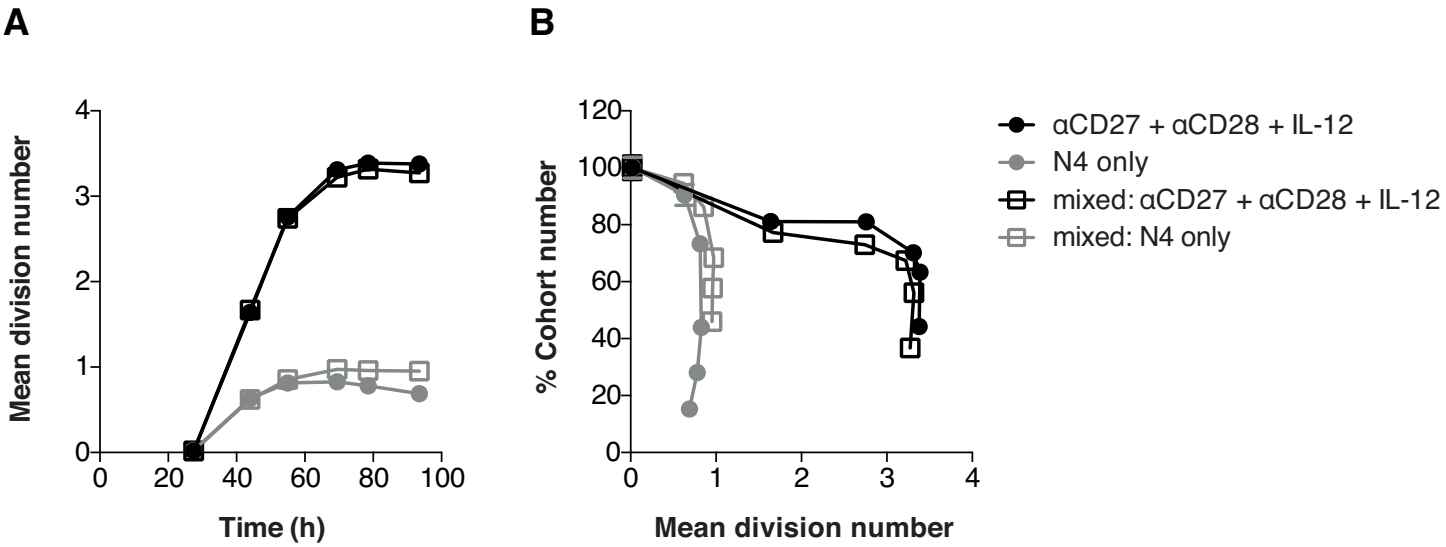

Fig. S6. Increase in DD programmed by combined costimuli is cell intrinsic.
(**A**) Mean division number and (**B**) percentage cohort number (refer to Fig. 2A and (*19*)) of OT-I/*Bcl2l11*$^{-/-}$ CD8^{+} T cells stimulated with N4 peptide and cultured without costimulation (CFSE labeled, grey lines) or with immobilized anti-CD27, anti-CD28 and IL-12 (CTV labeled, black lines, 5 μg/mL, 2 μg/mL, and 1 ng/mL respectively) for 26 hrs, washed and either cultured individually (solid circles) or co-cultured (open squares) without further costimulation. All cultures contained S4B6 at 25 μg/mL. Representative of 2 independent experiments, Mean ± SEM from triplicate culture wells.

A

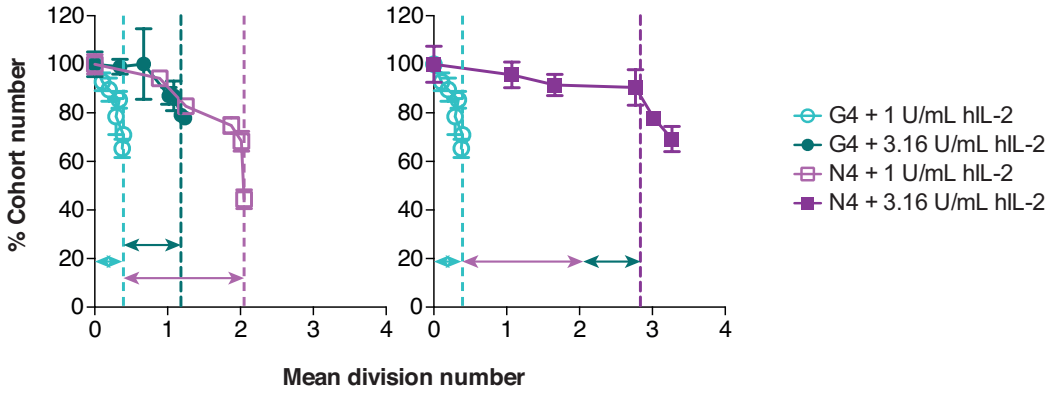
% Cohort number
Mean division number
G4 + 1 U/mL hIL-2
G4 + 3.16 U/mL hIL-2
N4 + 1 U/mL hIL-2
N4 + 3.16 U/mL hIL-2

B

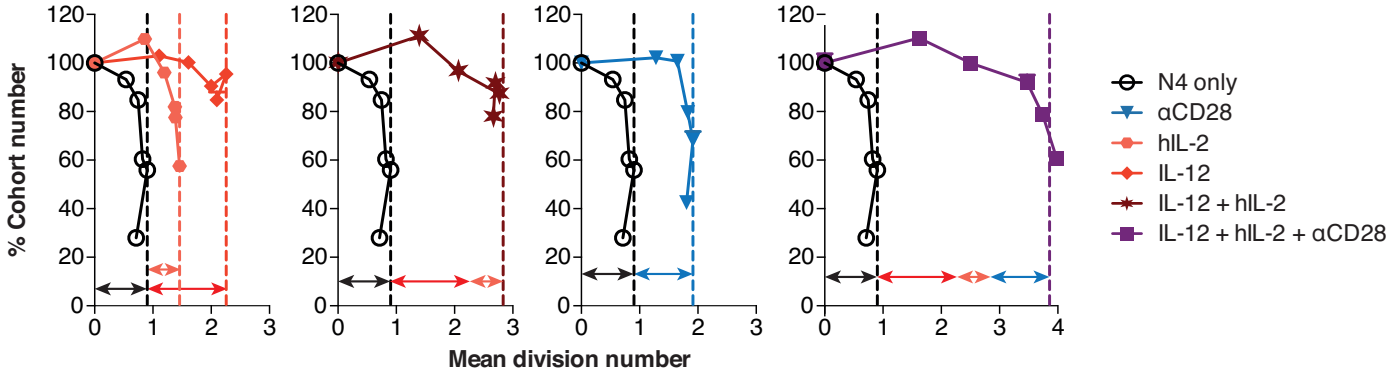
% Cohort number
Mean division number
N4 only
αCD28
hIL-2
IL-12
IL-12 + hIL-2
IL-12 + hIL-2 + αCD28

C

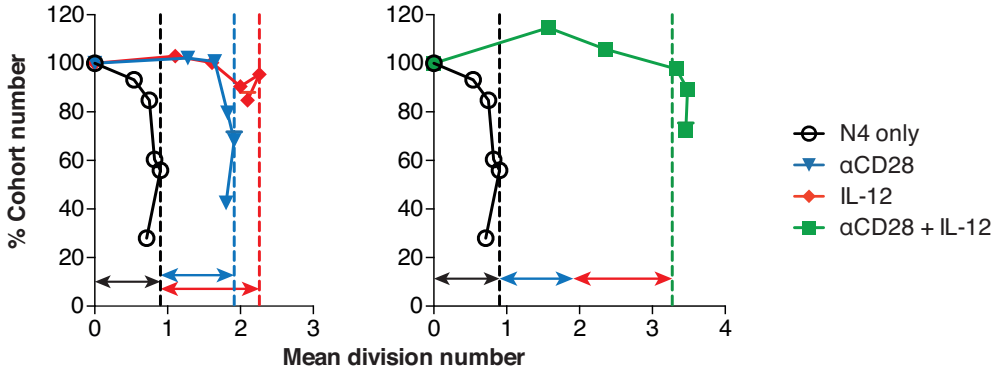
% Cohort number
Mean division number
N4 only
αCD28
IL-12
αCD28 + IL-12

D

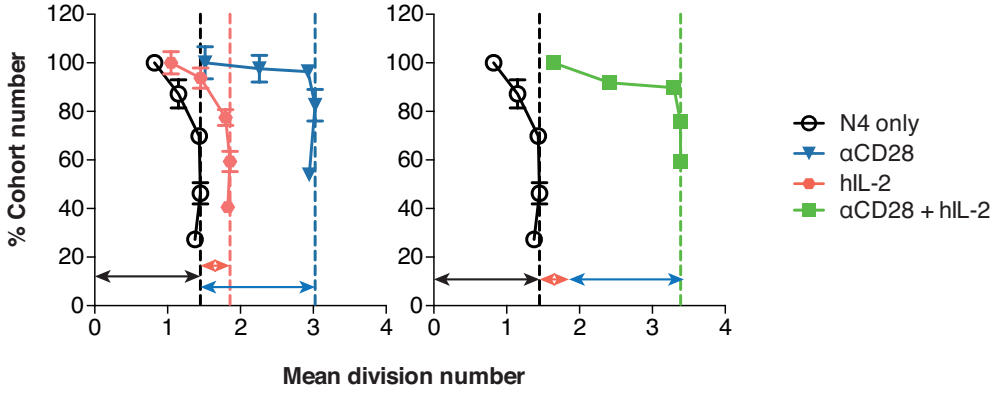
% Cohort number
Mean division number
N4 only
αCD28
hIL-2
αCD28 + hIL-2

Fig. S7. Summation of DD from multiple stimuli.
Percentage cohort number (refer to Fig. 2A and (*19*)) *vs.* mean division number for CTV-labeled OT-I/*Bcl2l11*$^{-/-}$ CD8^{+} T cells stimulated with (**A**) N4 (0.01 μg/mL for all cultures, K_d= 6.5 μM) or G4 (0.1 μg/mL, K_d= 10.0 μM) peptide in the presence of 3.16 or 1 U/mL hIL-2 or N4 peptide plus (**B**) IL-12, IL-2 and anti-CD28 (0.01 ng/mL, 1 U/mL and 0.63 μg/mL respectively for all cultures) (**C**) IL-12 and anti-CD28 and (**D**) IL-2 and anti-CD28 alone or in combination. Arrows represent the effect of individual stimuli on mDD. All cultures contained S4B6 at 25 μg/mL Graphs are representative of 2-3 independent experiments. Mean ± SEM from triplicate culture wells.

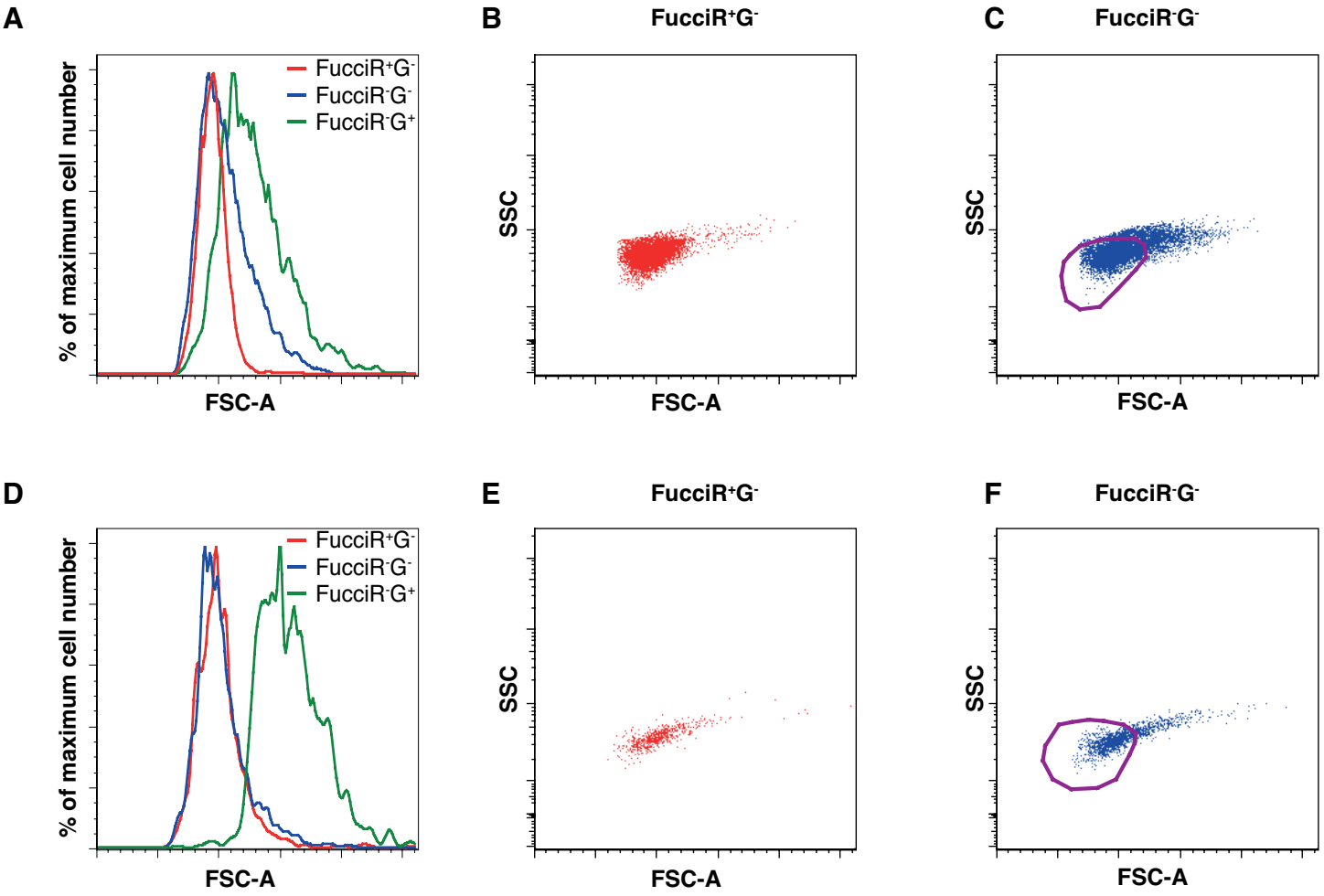

Fig. S8. Estimating quiescent cells from FucciR expression and cell size. Representative plots from (A-C) OT-I/FucciRG CD8$^+$ T cells transferred to HKx31-N4 infected recipients on day 2 post infection from the mLN day 5 post-transfer and (D-F) OT-I/FucciRG CD8$^+$ T cells stimulated for 91.5hrs with N4 *in vitro* in the presence of m-IL-2 blocking antibody, S4B6 and 3.16 U/mL hIL2. (**A, D**) FSC-A histogram of FucciR$^-$G$^+$ (red), FucciR$^-$G$^-$ (blue) and FucciR$^-$G$^+$ (green) T cells. Dot plots showing FSC-A *vs.* SSC-A for (**B, E**) FucciR$^+$G$^-$ T cells and (**C, F**) FucciR$^-$G$^-$ T cells. Quiescent cells were defined as being either FucciR$^+$G$^-$ (B, E) or FucciR$^-$G$^-$ and small (purple gate) (C,F). Plots are representative of 2 independent experiments.

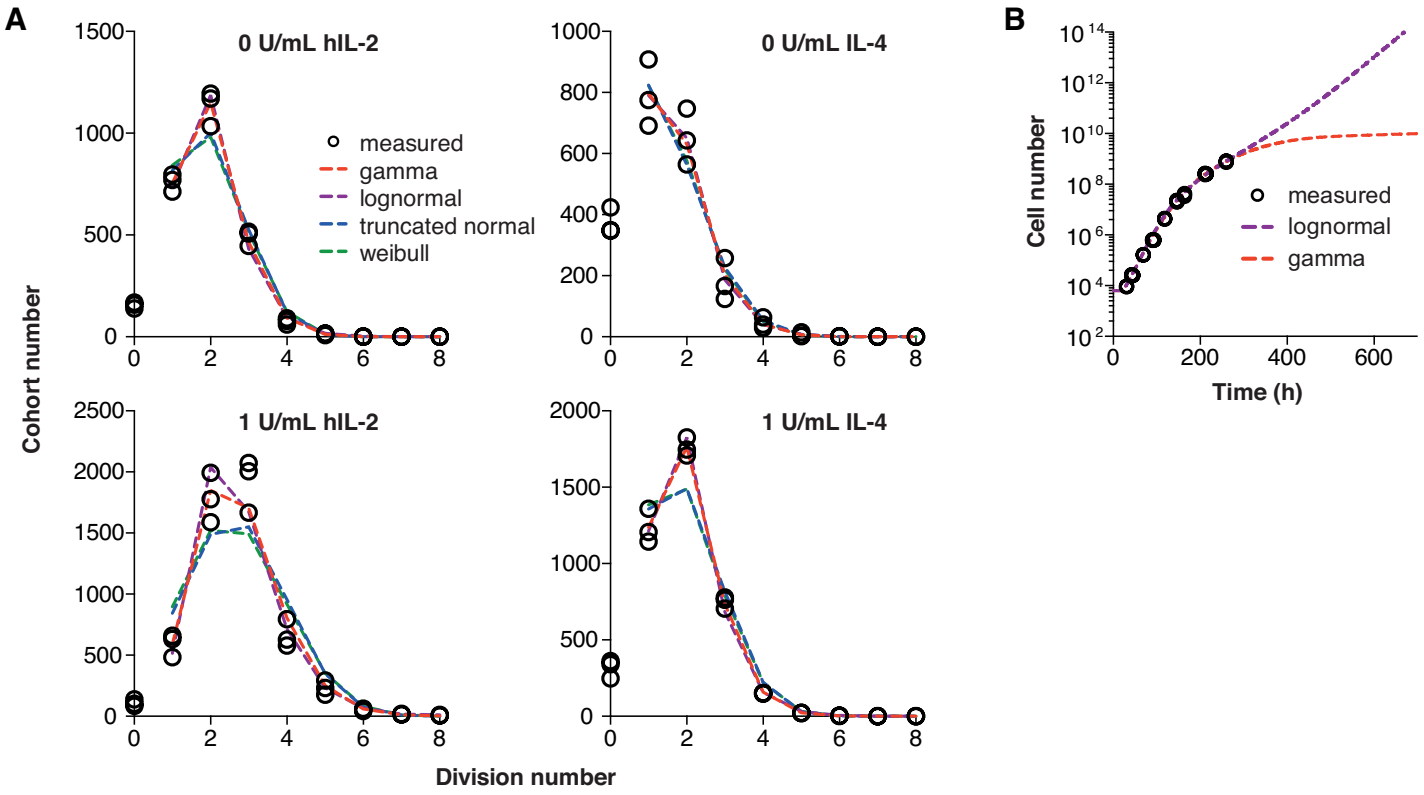

Fig. S9. The advantage of the discretized gamma distribution for describing DD. (**A**) Discretized truncated normal, lognormal, gamma and weibull distributions fit to cohort number per division of CTV labeled OT-I/*Bcl2l11*$^{-/-}$ CD8^{+} T cells stimulated with N4 and cultured in the presence of IL-2 (left) or IL-4 (right) at 0 (top) or 1 (bottom) U/mL for 89hrs, a time-point by which cells have reached DD. (**B**) CTV labeled OT-I/*Bcl2l11*$^{-/-}$ CD8^{+} T cells stimulated with N4 in the presence of 100 U/mL hIL-2 and sub-cultured into fresh medium containing cytokine every ~48 hrs. Cell number was fitted using the Cyton model with a discretized lognormal (purple) or discretized gamma distribution (red) for DD. Circles are technical replicates with mean of the best fits shown. Graphs are representative of 2 independent experiments.

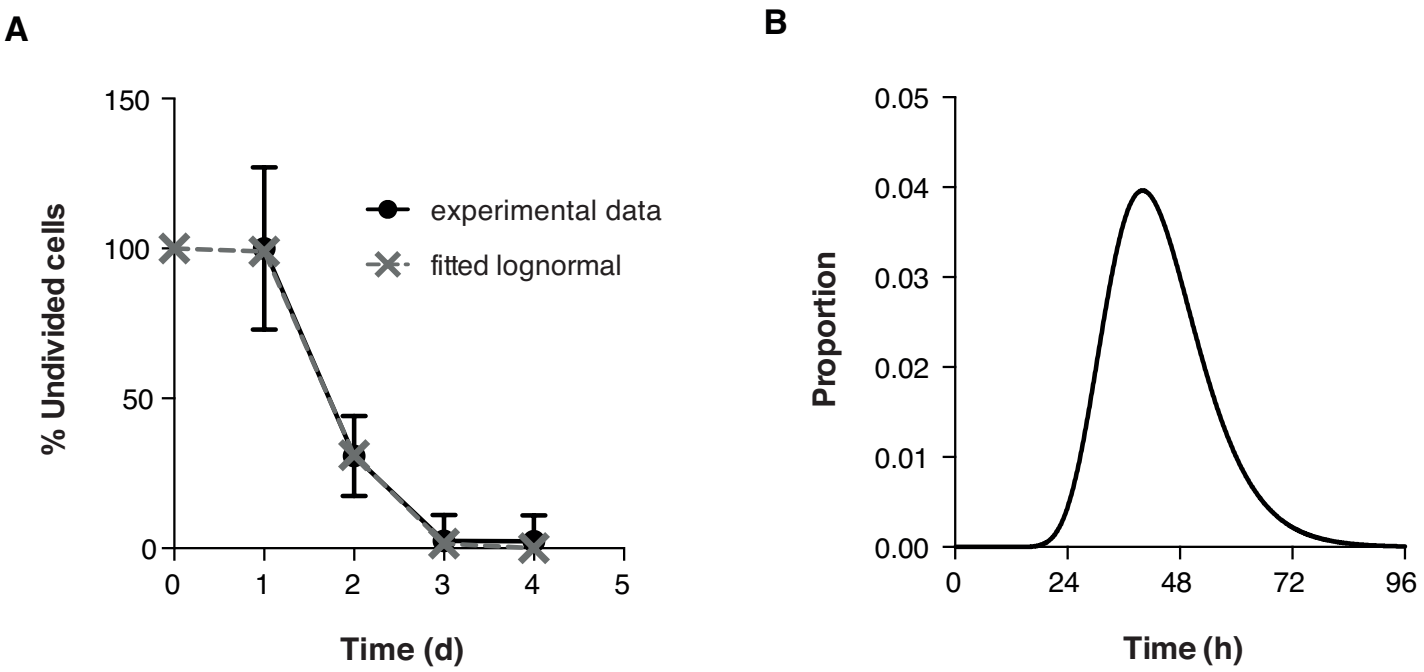

Fig. S10. Estimating mean time to first division for *in vivo* influenza infection.
10^5 CTV-labeled OT-I T cells were transferred into HKx31-N4 infected recipients 2 days post-infection and recovered from pooled mLN, spleen and lungs daily for days 1-7 post-transfer. Undivided cell numbers for days 5-7 were considered background and subtracted from undivided cell numbers measured on days 1-4. (A) Undivided cells at each time-point were percentage normalized to the number of undivided cells at day 1 post-transfer and fitted with an inverse cumulative lognormal distribution (grey line) to estimate the (B) best fit lognormal distribution describing time to first division (μ = 43.74 h, σ = 10.65 h). N= 5-7 mice/time-point pooled from 2 independent experiments: Mean ± SEM.

Table S1.
Cyton model best fit (±95% CI) to OT-I/FucciRG $CD8^+$ T cells from *in vivo* HKx31-N4 immune response or *in vitro* stimulation with N4 in the presence of S4B6. *

	N_0	μ_0^{div} (hrs)	σ_0^{div} (hrs)	μ_{1+}^{div} (hrs)	σ_{1+}^{div} (hrs)	μ_{1+}^{die} (hrs)	σ_{1+}^{die} (hrs)	μ^{DD}	σ^{DD}
in vivo EX1	1515 (1265, 3166)	43.74	10.65	5.78 (4.53, 6.84)	0.81	43.61 (10.42, 79.98)	40.81 (0.14, 75.86)	10.15 (7.39, 11.99)	2.39 (2.00, 3.19)
in vivo EX2	2102 (2102, 4453)								
in vitro	5000	29.09 (28.39, 29.56)	3.17 (2.65, 3.34)	7.13 (7.01, 7.61)	0.48 (0.35, 1.50)	11.39 (10.75, 11.75)	7.38 (6.52, 7.55)	3.58 (3.48, 3.71)	1.14 (1.04, 1.16)

Table S2.
Cyton model best fit (±95% CI) to OT-I/*Bcl2l11*$^{+/+}$ and OT-I/*Bcl2l11*$^{-/-}$ $CD8^+$ T cells stimulated with N4 in the presence of S4B6. *

	N_0	μ_0^{div} (hrs)	σ_0^{div} (hrs)	μ_{1+}^{div} (hrs)	σ_{1+}^{div} (hrs)	μ_{1+}^{die} (hrs)	σ_{1+}^{die} (hrs)	μ^{DD}	σ^{DD}
OT-I/ *Bcl2l11*$^{+/+}$	8641	32.33 (31.75, 32.82)	2.90 (2.28, 3.26)	5.95 (5.60, 6.29)	0.30 (0.28, 1.14)	10.04 (9.58, 10.32)	8.76 (7.94, 9.66)	2.60 (2.54, 2.73)	0.94 (0.89, 1.06)
OT-I/ *Bcl2l11*$^{-/-}$	11160	36.67 (36.42, 37.31)	5.35 (4.15, 5.09)	6.62 (5.83, 6.49)	0.33 (0.29, 1.21)	34.25 (33.68, 35.24)	24.93 (23.00, 26.28)	2.30 (2.28, 2.32)	0.76 (0.75, 0.77)

Table S3.
Cyton model best fit (±95% CI) to OT-I/*Bcl2l11*$^{-/-}$ CD8^{+} T cells stimulated with N4 peptide and sub-cultured with titrated hIL-2. *

[hIL-2] (U/mL)	N_0	μ_0^{div} (hrs)	σ_0^{div} (hrs)	μ_{1+}^{div} (hrs)	σ_{1+}^{div} (hrs)	μ_{1+}^{die} (hrs)	σ_{1+}^{die} (hrs)	μ^{DD}	σ^{DD}
316	6228	32.32 (32.02, 32.84)	9.26 (9.00, 10.01)	8.87 (8.80, 9.06)	1.25	77.92 (59.04, 94.88)	102.14 (0.77, 124.41)	12.85 (10.50, 14.92)	3.76 (3.52, 3.87)
100	6347					115.03 (110.16, 386.38)	1.15 (1.10, 507.82)	10.71 (10.46, 10.95)	3.58 (3.51, 3.63)
31.6	6219					32.92 (21.49, 114.12)	31.93 (6.65, 149.59)	15.73 (10.36, 16.00)	3.62 (3.27, 3.69)
10	6617					39.30 (38.18, 95.12)	51.52 (0.90, 69.88)	11.63 (6.27, 11.99)	3.99 (2.85, 4.00)
3.16	6429					40.90 (22.00, 247.39)	41.89 (19.36, 191.14)	5.43 (4.39, 5.58)	2.32 (2.05, 2.41)
1	6533					45.45 (38.34, 62.03)	33.65 (15.88, 54.24)	2.97 (2.58, 3.71)	1.61 (1.54, 1.73)
0.316	5612					36.25 (7.93, 204.29)	15.21 (0.08, 33.23)	2.40 (2.24, 2.99)	0.92 (0.59, 1.75)
0	5935					33.49 (7.52, 260.01)	0.40 (0.08, 50.16)	2.01 (1.69, 3.00)	0.70 (0.50, 0.95)

Table S4.
Cyton model best fit (±95% CI) to OT-I/*Bcl2l11*$^{-/-}$ CD8^{+} T cells stimulated with N4 peptide and sub-cultured with IL-4. *

[IL-4] (U/mL)	N_0	μ_0^{div} (hrs)	σ_0^{div} (hrs)	μ_{1+}^{div} (hrs)	σ_{1+}^{div} (hrs)	μ_{1+}^{die} (hrs)	σ_{1+}^{die} (hrs)	μ^{DD}	σ^{DD}
5000	6656	29.21 (28.52, 29.38)	3.66 (3.47, 3.74)	7.61 (7.51, 7.80)	1.07	56.70 (50.94, 65.85)	74.32 (66.77, 86.33)	9.78 (9.26, 10.29)	3.26 (3.17, 3.34)
1000	6557	29.20 (28.83, 32.26)	3.56 (3.49, 9.36)	7.64 (7.44, 8.24)	1.08	59.46 (53.83, 68.41)	77.94 (70.56, 89.72)	9.29 (8.91, 9.67)	3.18 (3.09, 3.25)
0	7808	35.13 (29.47, 39.03)	6.10 (2.91, 11.21)	7.38 (7.20, 9.40)	1.04	52.67 (50.87, 55.59)	61.74 (55.91, 72.70)	2.71 (2.69, 2.78)	0.84 (0.78, 0.86)

Table S5.
Cyton model best fit (±95% CI) to OT-I/*Bcl2l11*$^{-/-}$ CD8^{+} T cells stimulated for 26 hrs with N4 peptide and anti-CD28, immobilized anti-CD27 and IL-12 individually or in combination washed and replated with no further stimulation. *

Costim.	N_0	μ_0^{div} (hrs)	σ_0^{div} (hrs)	μ_{1+}^{div} (hrs)	σ_{1+}^{div} (hrs)	μ_{1+}^{die} (hrs)	σ_{1+}^{die} (hrs)	μ^{DD}	σ^{DD}
N4 only	6066	39.74 (38.54, 39.91)	5.94 (5.68, 6.26)	6.97 (6.83, 8.21)	0.35 (0.34, 0.41)	40.45 (39.26, 41.34)	35.64 (32.61, 38.05)	1.67 (1.66, 1.68)	0.58 (0.57, 0.60)
αCD28	8252	37.89 (35.63, 38.29)	5.84 (4.34, 6.16)	7.61 (7.39, 7.81)	0.38 (0.37, 0.39)	52.34 (51.24, 99.74)	44.01 (21.25, 46.84)	2.17 (1.93, 2.20)	0.77 (0.76, 0.80)
αCD27	8377	36.56 (31.90, 37.08)	5.39 (2.81, 5.58)	7.44 (7.30, 7.84)	0.37 (0.37, 0.39)	50.83 (49.83, 56.00)	42.22 (32.68, 45.55)	2.57 (2.41, 2.59)	0.67 (0.66, 0.72)
IL-12	8184	37.66 (36.89, 38.17)	4.68 (4.45, 4.81)	6.55 (6.35, 6.76)	0.33 (0.32, 0.34)	122.70 (98.55, 125.58)	160.83 (98.18, 164.62)	2.17 (2.15, 2.18)	0.92 (0.90, 0.93)
αCD28 + aCD27	8649	35.73 (35.38, 36.01)	5.41 (5.04, 5.77)	7.98 (7.88, 8.14)	0.40 (0.39, 0.41)	51.35 (50.41, 51.94)	29.28 (27.75, 31.48)	3.15 (3.13, 3.16)	0.76 (0.75, 0.77)
αCD28 + αCD27 + IL-12	7135	38.65 (38.36, 38.87)	4.77 (4.57, 4.95)	6.43 (6.33, 6.53)	0.32 (0.32, 0.33)	63.37 (61.61, 65.19)	45.14 (42.15, 49.05)	4.19 (4.16, 4.22)	1.04 (1.02, 1.05)

Table S6.
Cyton model best fit (±95% CI) to OT-I/*Il2ra*$^{+/+}$ and OT-I/*Il2ra*$^{-/-}$ CD8^{+} T cells co-transferred in equal numbers into HKx31-N4 or HKx31-Q4 infected recipient mice.*

	N_0	μ_0^{div} (hrs)	σ_0^{div} (hrs)	μ_{1+}^{div} (hrs)	σ_{1+}^{div} (hrs)	μ_{1+}^{die} (hrs)	σ_{1+}^{die} (hrs)	μ^{DD}	σ^{DD}
Q4 *Il2ra*$^{-/-}$	1148.00 (187.98, 1148.00)	43.74	10.65	6.15 (4.04, 6.44)	0.87	104.95 (53.45, 119.86)	89.17 (29.26, 152.39)	6.20 (4.35, 8.81)	0.99 (0.70, 2.02)
Q4 *Il2ra*$^{+/+}$								6.97 (4.90, 9.79)	1.48 (0.70, 2.22)
N4 *Il2ra*$^{-/-}$								8.85 (5.97, 10.68)	0.70 (0.70, 2.37)

Table S7.
Alternative DD distribution Cyton model fits to OT-I/*Bcl2l11*$^{-/-}$ CD8^{+} T cells stimulated in limiting conditions. †

condition		truncated normal	weibull	lognormal	gamma
0 U/mL hIL-2	mean	2.24	2.32	2.47	2.45
	st.dev.	1.05	0.97	0.80	0.80
	chi^2	157.38	186.21	45.70	13.42
1 U/mL hIL-2	mean	3.08	3.14	3.20	3.21
	st.dev.	1.35	1.28	1.06	1.07
	chi^2	1365.29	1394.46	249.24	217.48
0 U/mL IL-4	mean	1.28	1.87	2.16	2.09
	st.dev.	1.35	0.98	0.80	0.84
	chi^2	96.34	68.39	2.69	11.03
1 U/mL IL-4	mean	2.13	2.30	2.47	2.44
	st.dev.	1.16	1.02	0.82	0.83
	chi^2	355.79	342.73	41.97	6.03

Table S8.
Alternative DD distribution Cyton model fits to OT-I/*Bcl2l11*$^{-/-}$ CD8^{+} T cells maintained in hIL-2. *

	N_0	μ_0^{div} (hrs)	σ_0^{div} (hrs)	μ_{1+}^{div} (hrs)	σ_{1+}^{div} (hrs)	μ_{1+}^{die} (hrs)	σ_{1+}^{die} (hrs)	μ^{DD}	σ^{DD}
gamma	6396	32.34	9.59	8.93	1.26	115.48	1.15	10.85	3.57
log-normal	6396	32.34	9.59	8.93	1.26	115.48	1.15	11.4	3.16

Table S9.
Data from Table S3 fitted with different threshold factors. *

threshold value	N_0	μ_0^{div} (hrs)	σ_0^{div} (hrs)	μ_{1+}^{div} (hrs)	σ_{1+}^{div} (hrs)	μ_{1+}^{die} (hrs)	σ_{1+}^{die} (hrs)	μ^{DD}	σ^{DD}
0.25	8642	32.29	2.92	6.11	0.45	10.15	9.42	2.72	1.05
0.5	8642	32.29	2.92	6.11	0.45	10.15	9.42	2.72	1.05
1	8642	32.33	2.9	5.95	0.3	10.04	8.76	2.72	1.05
2	8642	32.34	2.9	5.93	0.3	9.99	8.58	2.72	1.05
4	8642	32.34	2.9	5.93	0.3	9.99	8.57	2.72	1.05
0.25	11161	36.69	5.27	6.57	0.48	34.33	24.92	2.3	0.77
0.5	11161	36.69	5.27	6.57	0.48	34.33	24.92	2.3	0.77
1	11161	36.67	5.35	6.62	0.33	34.25	24.93	2.3	0.77
2	11161	36.68	5.37	6.62	0.33	34.23	24.94	2.3	0.77
4	11161	36.68	5.37	6.62	0.33	34.23	24.94	2.3	0.77

* μ^{DD} and σ^{DD} for cyton fits are reported from the continuous gamma distributions. For plotting, these values are discretized as described in Supplementary Online Text.

† mean and standard deviation are reported from the discretized distributions.

References and Notes:

1. D. Zehn, S. Y. Lee, M. J. Bevan, Complete but curtailed T-cell response to very low-affinity antigen. *Nature* **458**, 211 (2009).
2. S. M. Kaech, R. Ahmed, Memory CD8+ T cell differentiation: initial antigen encounter triggers a developmental program in naïve cells. *Nat. Immunol.* **2**, 415 (2001).
3. M. J. van Stipdonk, E. E. Lemmens, S. P. Schoenberger, Naïve CTLs require a single brief period of antigenic stimulation for clonal expansion and differentiation. *Nat. Immunol.* **2**, 423 (2001).
4. E. M. Bertram, W. Dawicki, T. H. Watts, Role of T cell costimulation in anti-viral immunity. *Sem. Immunol.* **16**, 185 (2004).
5. J. M. Curtsinger *et al.*, Inflammatory cytokines provide a third signal for activation of naive CD4+ and CD8+ T cells. *J. Immunol.* **162**, 3256 (1999).
6. A. G. Baxter, P. D. Hodgkin, Activation rules: the two-signal theories of immune activation. *Nat. Rev. Immunol.* **2**, 439 (2002).
7. D. A. Cantrell, K. A. Smith, The interleukin-2 T-cell system: a new cell growth model. *Science* **224**, 1312 (1984).
8. L. A. Gravestein, J. D. Nieland, A. M. Kruisbeek, J. Borst, Novel mAbs reveal potent co-stimulatory activity of murine CD27. *Int. Immunol.* **7**, 551 (1995).
9. F. A. Harding, J. G. McArthur, J. A. Gross, D. H. Raulet, J. P. Allison, CD28-mediated signalling co-stimulates murine T cells and prevents induction of anergy in T-cell clones. *Nature* **356**, 607 (1992).
10. T. R. Malek, The biology of interleukin-2. *Annu. Rev. Immunol.* **26**, 453 (2008).
11. A. Oxenius, U. Karrer, R. M. Zinkernagel, H. Hengartner, IL-12 Is Not Required for Induction of Type 1 Cytokine Responses in Viral Infections. *J. Immunol.* **162**, 965 (1999).
12. A. Shahinian *et al.*, Differential T cell costimulatory requirements in CD28-deficient mice. *Science* **261**, 609 (1993).
13. K. P. J. M. van Gisbergen *et al.*, The costimulatory molecule CD27 maintains clonally diverse CD8(+) T cell responses of low antigen affinity to protect against viral variants. *Immunity* **35**, 97 (2011).
14. E. D. Hawkins, J. F. Markham, L. P. McGuinness, P. D. Hodgkin, A single-cell pedigree analysis of alternative stochastic lymphocyte fates. *Proc. Natl. Acad. Sci. U.S.A* **106**, 13457 (2009).
15. E. D. Hawkins, M. L. Turner, M. R. Dowling, C. van Gend, P. D. Hodgkin, A model of immune regulation as a consequence of randomized lymphocyte division and death times. *Proc. Natl. Acad. Sci. U.S.A* **104**, 5032 (2007).
16. M. L. Turner, E. D. Hawkins, P. D. Hodgkin, Quantitative regulation of B cell division destiny by signal strength. *J. Immunol.* **181**, 374 (2008).

17. M. R. Dowling *et al.*, Stretched cell cycle model for proliferating lymphocytes. *Proc. Natl. Acad. Sci. U.S.A* **111**, 6377 (2014).

18. M. Tomura *et al.*, Contrasting quiescent G0 phase with mitotic cell cycling in the mouse immune system. *PLoS ONE* **8**, e73801 (2013).

19. Materials and methods are available as supplementary materials on Science Online.

20. A. E. Denton *et al.*, Affinity thresholds for naive CD8+ CTL activation by peptides and engineered influenza A viruses. *J. Immunol.* **187**, 5733 (2011).

21. E. D. Hawkins *et al.*, Quantal and graded stimulation of B lymphocytes as alternative strategies for regulating adaptive immune responses. *Nat. Commun.* **4**, 2406 (2013).

22. V. R. Buchholz *et al.*, Disparate Individual Fates Compose Robust CD8+ T Cell Immunity. *Science* **340**, 630 (2013).

23. C. Gerlach *et al.*, Heterogeneous Differentiation Patterns of Individual CD8+ T Cells. *Science* **340**, 635 (2013).

24. M. Hommel, P. D. Hodgkin, TCR affinity promotes CD8+ T cell expansion by regulating survival. *J. Immunol.* **179**, 2250 (2007).

25. E. K. Deenick, A. V. Gett, P. D. Hodgkin, Stochastic model of T cell proliferation: a calculus revealing IL-2 regulation of precursor frequencies, cell cycle time, and survival. *J. Immunol.* **170**, 4963 (2003).

26. As OT-I division times are relatively homogeneous a division based dilution model is difficult to distinguish from a mechanism where the loss of division motivation ceases in all descendants at a nominated time after activation. Further molecular studies are needed to test between these, and other possible mechanisms.

27. W. Weninger, M. A. Crowley, N. Manjunath, U. H. von Andrian, Migratory Properties of Naive, Effector, and Memory CD8+ T Cells. *J. Exp. Med.* **194**, 953 (2001).

28. M. Dougan, G. Dranoff, Immune therapy for cancer. *Annu. Rev. Immunol.* **27**, 83 (2009).

29. G. Kinnear, N. D. Jones, K. J. Wood, Costimulation blockade: current perspectives and implications for therapy. *Transplantation* **95**, 527 (2013).

30. G. T. Belz, L. Zhang, M. D. H. Lay, F. Kupresanin, M. P. Davenport, Killer T cells regulate antigen presentation for early expansion of memory, but not naive, CD8+ T cell. *Proc. Natl. Acad. Sci. U.S.A* **104**, 6341 (2007).

31. M. Liu, M. E. Shapiro, A new method for isolation of murine islets with markedly improved yields. *Transplant. Proc.* **27**, 3208 (1995).

32. V. G. Subramanian, K. R. Duffy, M. L. Turner, P. D. Hodgkin, Determining the expected variability of immune responses using the cyton model. *J. Math. Biol.* **56**, 861 (2008).